water

Article

Synthesis and Characterization of Potassium Bicarbonate and Urea-Modified Biochar from Rape Straw: Application in the Removal of Tetracycline from Aqueous Solution

Zhipeng Zhang [1,2], Chenghan Tang [3], Hongbin Wang [4], Ming Zhong [5], Pengchao Ge [6], Wenlai Xu [7] and Yiyang Chen [8,*]

[1] Sichuan Geological Environment Survey and Research Center, Chengdu 610081, China; zzpwss123@126.com
[2] Engineering & Technology Center of Groundwater Pollution Control for Environmental Protection in Sichuan, Chengdu 610081, China
[3] College of Environmental Science and Engineering, Southwest Jiaotong University, Chengdu 611756, China; 15201822120@163.com
[4] Sichuan Provincial Engineering Research Center of City Solid Waste Energy and Building Materials Conversion and Utilization Technology, Chengdu 610199, China; wanghongbin@cdu.edu.cn
[5] National Postdoctoral Research Station, Haitian Water Group, Chengdu 610213, China; txgsfy@163.com
[6] School of Materials and Environmental Engineering, Chengdu Technological University, Chengdu 611730, China; 15582326457@163.com
[7] College of Ecology and Environment, Chengdu University of Technology, Chengdu 610059, China; xuwenlai2012@cdut.cn
[8] Sichuan Ecology and Environment Industry Group Co., Ltd., Chengdu 610095, China
* Correspondence: chenyiyang@sdholding.com; Tel.: +86-13880902258

Abstract: Using rapeseed straw as a raw material and potassium bicarbonate ($KHCO_3$) and urea ($CO(NH_2)_2$) as modification reagents, the pyrolysis raw materials were mixed in a certain proportion, and the unmodified biochar GBC800, $KHCO_3$-modified biochar KGBC800, and $(KHCO_3)/(CO(NH_2)_2)$ co-modified biochar N-KGBC800 were, respectively, prepared using the one-pot method at 800 °C. The physicochemical properties, such as surface morphology, pore characteristics, functional group distribution, and elemental composition of the three biochars, were characterized, and the adsorption performance and mechanism of the typical antibiotic tetracycline (TC) in water were studied. The results showed that the surface of GBC800 was smooth and dense, with no obvious pore structure, and both the specific surface area and total pore volume were small; the surface of KGBC800 showed an obvious coral-like three-dimensional carbon skeleton, the number of micropores and the specific surface area were significantly improved, and the degree of carbonization and aromatization was enhanced; N-KGBC800 had a coral-like three-dimensional carbon skeleton similar to KGBC800, and there were also many clustered carbon groups. The carbon layer changed significantly with interlayer gaps, presenting a multi-level porous structure. After N doping, the content of N increased, and new nitrogen-containing functional groups were formed. When the initial TC concentration was 100 mg/L, pH $\approx$ 3.4, the temperature was 25 °C, and the dosage of the three biochars was 0.15 g/L, the adsorption equilibrium was reached before 720 min. The adsorption capacities of GBC800, KGBC800, and N-KGBC800 for TC were 16.97 mg/g, 294.86 mg/g, and 604.71 mg/g, respectively. Fitting the kinetic model to the experimental data, the adsorption of TC by the three biochars was more in line with the pseudo-second-order adsorption kinetic model, and the adsorption isotherm was more in line with the Langmuir model. This adsorption process was a spontaneous endothermic reaction, mainly chemical adsorption, specifically involving multiple adsorption mechanisms such as pore filling, electrostatic attraction, hydrogen bonds, $n-\pi$ interaction, Lewis acid–base interaction, $\pi-\pi$ stacking, or cation $-\pi$ interaction between the aromatic ring structure of the carbon itself and TC. A biochar-adsorption column was built to investigate the dynamic adsorption process of tetracycline using the three biochars against the background of laboratory pure water and salt water. The adsorption results show that the Thomas model and the Yoon–Nelson model both provide better predictions for dynamic adsorption processes. The modified biochars KGBC800 and N-KGBC800 can be used as preferred materials for the efficient adsorption of TC in water.

Citation: Zhang, Z.; Tang, C.; Wang, H.; Zhong, M.; Ge, P.; Xu, W.; Chen, Y. Synthesis and Characterization of Potassium Bicarbonate and Urea-Modified Biochar from Rape Straw: Application in the Removal of Tetracycline from Aqueous Solution. *Water* **2024**, *16*, 2522. https://doi.org/10.3390/w16172522

Academic Editor: Laura Bulgariu

Received: 26 July 2024
Revised: 29 August 2024
Accepted: 2 September 2024
Published: 5 September 2024

Keywords: biochar; potassium bicarbonate modification; nitrogen doping; tetracycline; adsorption mechanism

1. Introduction

China has a huge population and a strong demand for agricultural products. In 2021, China's grain output was 682.85 million tons, and the output of rice, wheat, corn, rapeseed, etc. accounted for about 20% of the global output [1]. Rapeseed is a major crop in China's oil economy [2]. In 2021, the output of rapeseed straw in China was approximately 29.147 million tons, the total amount of straw collected reached 23.684 million tons, and the comprehensive utilization amount was 20.591 million tons [3]. According to the statistics from the National Grain and Oils Information Center, by 2025, the planting area of rapeseed in China will reach about 80 million hectares. At that time, along with the planting and processing of rapeseed, its straw output will increase rapidly. The "14th Five-Year Plan for the Development of Circular Economy" clearly states that it is necessary to strengthen the resource utilization of wastes in the agricultural production process and promote the efficient utilization of agricultural and forestry wastes, such as crop straws, livestock and poultry manure, forestry wastes, and by-products of agricultural product processing [4]. In recent years, the resource utilization technologies of agricultural wastes at home and abroad and related research have significantly developed. In addition to the conventional "five utilization methods", namely, fertilization, feed utilization, combustion, substrate utilization, and raw material utilization. There are also deep processing and transformation technologies, such as solidification utilization technology, gasification utilization, and liquefaction utilization technology. The former has the disadvantage of a low utilization degree, while the latter has high requirements for equipment and technology and is difficult to popularize [5]. Therefore, exploring the efficient utilization of rapeseed straw has become the only way to support the sustainable development of the rapeseed industry.

Tetracycline (TC), an antibiotic with a strong antibacterial effect, low cost, and low allergenicity, is widely used in human health, animal disease control, and feed additives. China is the country with the largest production and usage of tetracycline worldwide [6]. Meanwhile, due to China's aquaculture area and aquatic product output accounting for more than 60% of the global total, according to the "2022 National Fishery Economic Statistics Bulletin", the national aquaculture area reached 7,107,500 hm^2, including 2,074,420 hm^2 of marine aquaculture area and 5,033,080 hm^2 of freshwater aquaculture area [7,8]. A large amount of tetracycline is used in the breeding process. Tetracycline is difficult for humans and animals to absorb. About 70–90% is discharged into water bodies or soil through urine and feces. Tetracycline is difficult to degrade in the natural environment, has poor biodegradability, and can also induce the production of resistant microorganisms and resistance genes, leading to serious biological environmental pollution and endangering public health [9]. Currently, the main methods for removing tetracycline from water include advanced oxidation methods [10], biological treatment methods [11], and adsorption methods [12]. Among them, the adsorption method has the advantages of low cost, simplicity, efficiency, and no harmful by-products and is considered one of the most effective wastewater treatment methods [13]. The original biochar has problems such as poor anti-interference ability and unsatisfactory adsorption capacity. Activation and modification can effectively improve the adsorption performance of biochar. Du et al. [14] prepared ginkgo biochar through ball mill modification, and its adsorption capacity for target pollutant increased from 16.47 mg/g to 182.63 mg/g; Zhang et al. [15] used corn cob waste as the experimental raw material and KOH as the modified activator. The adsorption capacity of CBC750 prepared for TC was three times that of ordinary biochar CBC. Sun et al. [16] prepared modified biochar with KOH and $FeCl_3$ to adsorb sulfonamide antibiotics in water. The maximum adsorption capacities for sulfadiazine, sulfamethazine, and sulfamethoxazole were 294.12 mg/g, 400.00 mg/g, and 454.55 mg/g, respectively, which were 5–7 times that of ordinary biochar. The nitrogen-doped biochar prepared by using bagasse as the carbon source, melamine as the nitrogen source, and sodium bicarbonate as the pore-forming agent was proved by Che et al. [17] to be a reliable wastewater treatment technology for adsorbing ciprofloxacin (CIP). In recent years, heteroatom doping has attracted much attention in improving the adsorption properties of carbon-based materials. For example, Lu et al. [18] used cellulose and ammonium oxalate to synthesize nitrogen-doped biochar with a layered porous structure, which enhanced the adsorption of toluene. Li et al. [19] prepared nitrogen-doped biochar with corn and urea for CO_2 adsorption, and studied that the introduction of surface N contributes to the generation of ultrafine pores. At the same time, since N has lone pair electrons and high electronegativity, the flow of π electrons in sp^2C is enhanced through conjugation, resulting in more abundant functional groups and surface defects [20,21]. Among the many current adsorbents, there are few studies on modifying rapeseed straw to remove TC in water, and its adsorption behavior characteristics and mechanism are still unclear.

Given this, this study aims to use rapeseed straw as the biomass raw material, potassium bicarbonate ($KHCO_3$) as the activator, and urea ($CO(NH_2)_2$) as the nitrogen source to prepare modified rapeseed straw biochar via one-pot oxygen-limited pyrolysis at 800 °C. The possibility and influencing factors of its application in the removal of TC from water bodies are discussed, and its adsorption mechanism is analyzed by combining kinetics, adsorption isotherms, thermodynamic models, and characterization methods. This provides a new and effective method for using rapeseed straw and efficiently removing TC from water.

2. Materials and Experimental Methods

2.1. Reagents and Apparatus Used in the Experiment

2.1.1. Test Reagents

Tetracycline hydrochloride, $KHCO_3$, urea, ethanol, HCl, NaOH, NaCl, $MgCl_2$, Na_2S, and $CaCl_2$ are analytically pure and were purchased from Cologne (Chengdu) Chemical Co.

2.1.2. Laboratory Instruments

The main instruments and equipment used in the experiment include the following: an ultraviolet–visible spectrophotometer (WFZ UV-4802, Shanghai, China), constant temperature oscillation incubator (BS-2E, Changzhou, Jiangsu, China), tube furnace (BEQ-1200C, Hefei, Anhui, China), precision bench top pH meter (pH S-3CU, Shanghai, China), analytical balance (FA224, Shanghai, China), electric blast drying oven (DHG-9240A, Shanghai, China), high-speed multifunctional crusher (SS-1022, Changzhou, Jiangsu, China), UPU ultrapure water system (UPHW-IV-90T, Chengdu, Sichuan, China), peristaltic pump (BT-100F, Baoding, HeBei, China), numerical control ultrasonic cleaner (CR-080S, Shenzhen, China), automatic sampler (CBS-A, Shanghai, China), scanning electron microscope (ZEISS Gemini SEM 300, Baden-Württemberg, Germany), BET-specific surface area analyzer (Quantachrome/ASiQwin, Boynton Beach, CA, USA), Fourier transform infrared spectrometer (Thermo Scientific Nicolet iS5, Waltham, MA, USA), and X-ray photoelectron spectrometer (Thermo Scientific K-Alpha, Waltham, MA, USA).

2.2. Preparation of Biochar

Experimental materials: rape straw from a farm in Pidu District, Chengdu City, Sichuan Province.

The process of biochar production using rapeseed straw is shown in Figure 1.

Using rape straw as the raw material for pyrolysis to produce biochar, after removing impurities such as stones and leaves, the straw was crushed using a crusher to pass through a 100-mesh sieve for sieving. An appropriate amount of the material was weighed and mixed at a ratio of biomass of $KHCO_3$:urea = 1:1.5:1 and then sent into a tube furnace purged with nitrogen for pyrolysis. The heating rate was 8 °C/min, the nitrogen flow rate was 50 mL/min, and the isothermal pyrolysis lasted 120 min. After the pyrolysis, the heating was stopped until it cooled to below 100 °C before removing it. The pyrolysis product was mixed with 1 mol/L HCl at a solid–liquid ratio of 1:10 (g:mL), and ultrasonic cleaning was performed for 15 min. Then, ultrapure water was added for cleaning, and this process was repeated multiple times until the pH of the supernatant was approximately 7 and remained stable. The resulting solid was collected, dried at 75 °C to a constant weight, and then ground using a ceramic mortar and passed through a 100-mesh sieve to ensure that the particle size of the material remained basically constant. After sieving, the solid was collected to obtain the modified biochar. That created without adding potassium bicarbonate and urea was named GBC800, the biochar with only potassium bicarbonate added was named KGBC800, and the one with both potassium bicarbonate and urea added was named N-KGBC800 biochar.

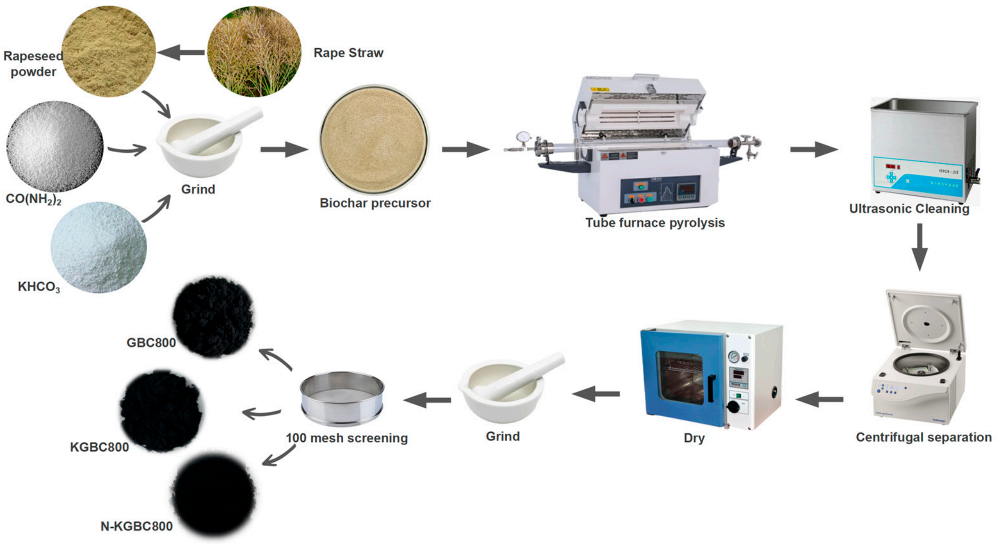

Figure 1. A flow chart of modified biochar preparation.

2.3. Adsorption Experiment

2.3.1. Batch Adsorption Experimental Method

First, a 1 g/L TC stock solution was prepared, which can be diluted to the required concentration of TC reaction solution as needed. Then, 200 mL of TC solution with a concentration of ρ_0 mg/L was taken and added to a 250 mL conical flask. Then, m g of GBC800, KGBC800, and N-KGBC800 was weighed and added. The original pH of the reaction solution was 3.4 (when exploring the effect of different pH on the adsorption performance of biochar, 1 mol/L of NaOH and HCl were used to change the pH of the solution). The solution was shaken in the dark at T °C and 150 r/min for t min. After the reaction, it was taken out and left to stand. A 5 mL syringe was used to draw 2 mL of the supernatant, and the biochar particles are filtered out through a 0.45 filter membrane. The filtrate was placed in a colorimetric tube containing 2 mL of pure water and stored at a low temperature for later use to determine its absorbance with an ultraviolet–visible spectrophotometer. When investigating the effect of the initial pH of the solution, ρ_0, m, T, and t were fixed at 100 mg/L, 0.15 g/L, 25 °C, and 720 min, respectively, and the pH = 3~11. When investigating the effect of the biochar dosage, ρ_0, pH, T, and t were fixed at 100 mg/L, 3.4, 25 °C, and 720 min, respectively, and the variation range of m was 0.05 to 0.4 g/L. When investigating the effect of the reaction time, ρ_0, m, pH, and T were fixed at 100 mg/L, 0.15 g/L, 3.4, and 25 °C, respectively, and the t values were 0, 5, 10, 20, 40, 70, 120, 180, 240, 360, 480, 600, and 720 min. Kinetic analysis was conducted based on the adsorption experimental data under different t values. When investigating the effect of the initial TC concentration of the solution and the reaction temperature, ρ_0, m, and pH were fixed at 100 mg/L, 0.15 g/L, and 3.4, respectively. The temperature varied at 15, 25, and 35 °C, and the initial concentrations of TC were 10, 20, 30, 40, 50, 60, 70, 80, 90, and 100 mg/L.

Adsorption isotherm models and adsorption thermodynamic analysis were conducted based on the experimental results.

2.3.2. Biochar Fixed-Bed Adsorption Experiment

The laboratory apparatus is illustrated in Figure 2. The chromatography column had an inner diameter of 10 mm and a length of 200 mm, and the filling sequence from bottom to top was 2.0 g of 30-mesh quartz sand, 0.1 g of biochar, and 8 g of 30-mesh quartz sand. A certain amount of TC sample was weighed and added to the brine (according to the mass ratio of NaCl (2.5%), MgCl (1.1%), $NaSO_4$ (0.4%), and $CaCl_2$ (0.16%)) to obtain simulated saline wastewater contaminated with TC (100 mg/L) as the reaction solution to be reacted. The conductor entered the tank through the worm pump, adsorption column, and automatic collector connection. The flow rate was adjusted to 2.0 mL/min of the reagent from the bottom up through the absorption column. The sampling time interval was 10 min, and the response time was 12 h. At the end of the reaction, the absorption rate was determined using an ultraviolet spectrometer to calculate the outflow concentration of TC.

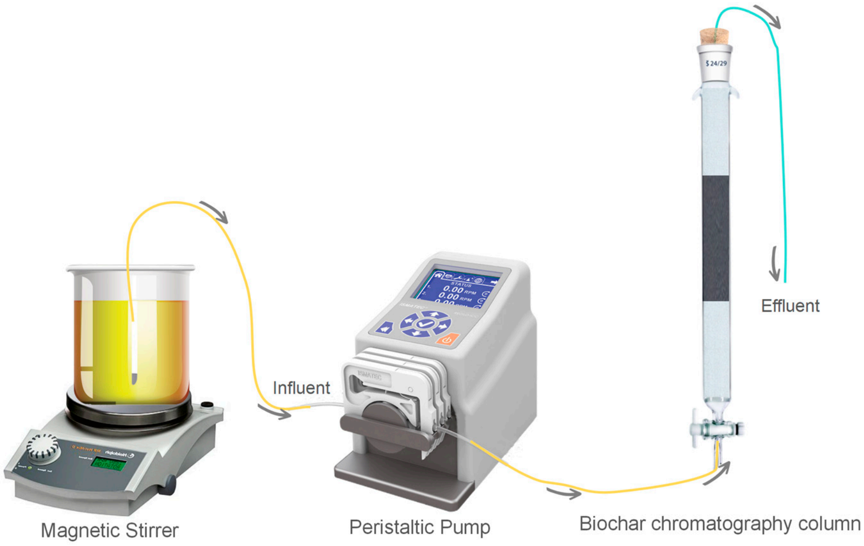

Figure 2. The biochar fixed-bed adsorption experimental device.

2.4. *UV-Vis Spectrophotometric Analysis of Tetracycline*

The detection method for TC: The absorbance of TC was 358 nm and was tested using a UV–visible spectrophotometer. The formula for calculating the adsorption capacity is shown below:

$$q_t = \frac{(C_0 - C_t) \times V}{m} \quad (1)$$

q_t is the adsorption capacity at time t, mg/g; C_0 is the initial concentration of the pollutant, mg/L; C_t is the concentration of the pollutant in the solution after a specific time of adsorption, mg/L; m is the amount of adsorbent dosing, g; and V is the volume of adsorbent solution, L.

3. Results and Discussion

3.1. *Material Characterization Results*

3.1.1. Analysis of Physical Properties of Materials

GBC800, KGBC800, and N-KGBC800 were placed under a scanning electron microscope to observe their structural features and microscopic patterns; the findings are displayed in Figure 3.

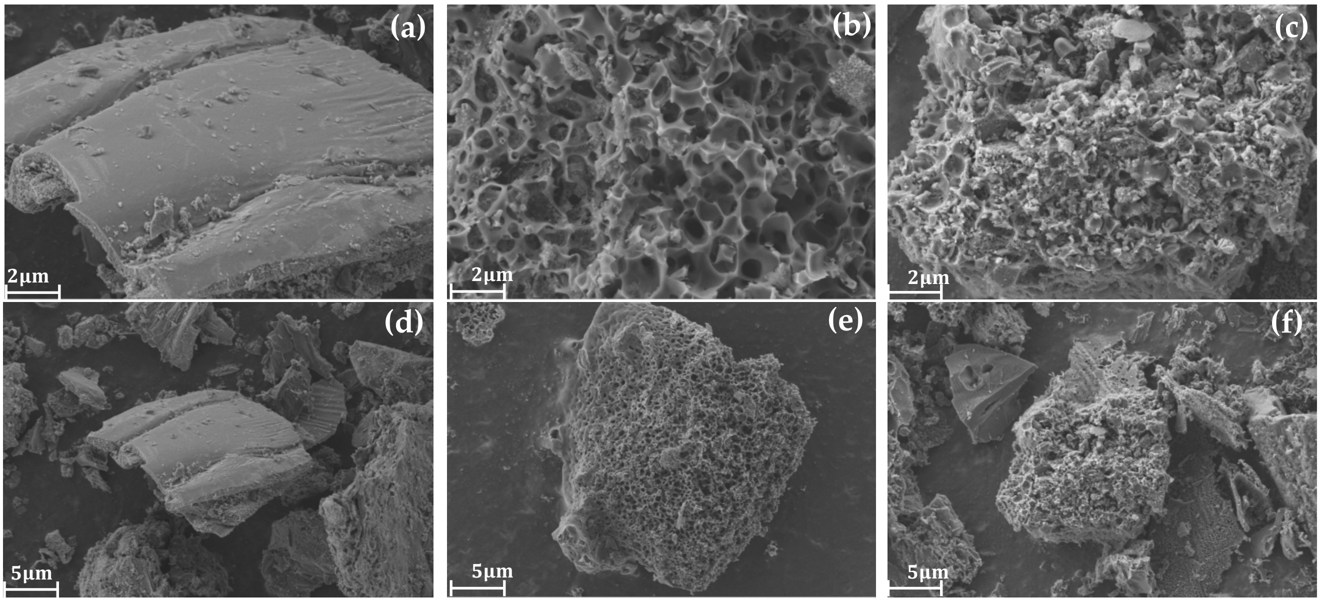

Figure 3. Scanning electron microscope images of biochar. (**a**,**d**) show the surface morphology of GBC800, (**b**,**e**) show the surface morphology of KGBC800, and (**c**,**f**) show the surface morphology of N-KGBC800.

In Figure 3a,d demonstrate the surface morphology of pristine rapeseed straw biochar GBC800 without activation and heteroatom doping, which has a smooth and compact surface without obvious pores and exhibits a dense carbon skeleton laminar structure with no obvious pores present at the edge fracture.

The morphology of KGBC800 prepared by $KHCO_3$ activation pyrolysis is shown in Figure 3b,e, which exhibits an obvious pore structure on the carbon surface, with a randomly generated coral-like carbon skeleton similar to a sphere and more extremely small pores on the surface. This is because the gas generated by the thermal decomposition of $KHCO_3$ will continuously impact the surface of the biochar to make it more uneven. At the same time, the thermal decomposition of K_2CO_3 generated by the heat into the cellulose weakens the intermolecular hydrogen bonding within the straw, making the biomass structure more easily damaged and forming a richer microporous structure. Around 700~800 °C, elemental K reacts with C to produce metal K, thereby continuing to etch the pore structure [22]. The vapor precipitation of potassium metal squeezes into the carbon interlayer to promote the activation reaction, forming a richer multilevel pore structure and a larger specific surface area, presenting a continuous sheet of a spherical, coral-like, three-dimensional pore structure [23].

Figure 3c,f demonstrate the surface morphology of N-KGBC800 prepared in the case of $KHCO_3$ activation and $CO(NH_2)_2$ doping, which exhibits a more complete stacked structure with the same spherical coral-like pore structure as that of KGBC800, with the pore sizes exhibiting a more irregular and inhomogeneous shape and the presence of a certain thickness of gaps between its carbon layers, generating more fine particles and pore channels. A two-dimensional network is generated between urea and H_2O due to strong hydrogen bonding, and $KHCO_3$ and $CO(NH_2)_2$ molecules can enter the pores and thermally decompose inside to form more micropores [24]. In addition, there are many fine massive carbon layers with rough outer surfaces and extremely tiny cluster structures on the surface, which may be formed due to chemical vapor deposition during the activation process. At around 320 °C, urea can decompose into HCNO and NH_3 [25,26]. NH_3 reacts chemically with the hydroxyl and carboxyl groups on the surface of the carbon layer to produce nitrogen-containing functional groups such as $-CO-NH_2$, $-C-NH_2$, etc. [27]. When the pyrolysis temperature exceeds 500 °C, NH_3 begins to decompose continuously, producing all kinds of chemical groups, which attack carbon-active sites on the surface of the biochar, leading to the formation of a larger surface area and a slight increase in the volume of micropores of the modified biochar [24,28].

N_2 adsorption/desorption was performed on all three biochars at a temperature of 77.3 K. The results are presented in Figure 4, and the parameters are presented in Table 1. With the addition of $KHCO_3$ and urea, the specific surface area and total pore volume of the biochar were significantly enhanced and clearly differentiated, with the specific surface area of N-KGBC800 being 1.4 and nearly 180 times higher than that of KGBC800 and GBC800, respectively, and the total pore volume being 1.3 and 26 times higher than that of KGBC800 and GBC800, respectively. The specific surface area and the total pore volume of GBC800 were small, and the overall pores were dominated by mesopores. However, it is noteworthy that the volume of micropores of KGBC800 was larger than that of N-KGBC800, and in general, the introduction of urea, to a certain extent, should open up the micropores inside the biochar even further. However, the microporous volume of N-KGBC800 decreases instead. This is mainly because the carbon layer, under the impact of CO_2 and NH_3 and the etching of metallic potassium monomers, undergoes a vaporization reaction with tiny potassium-containing compound crystals as the core, which cracks the surrounding carbon-containing compounds and swells the micropores into medium- or large-sized pores or leads to the loosening of its layers and fragility, which triggers the pore collapses.

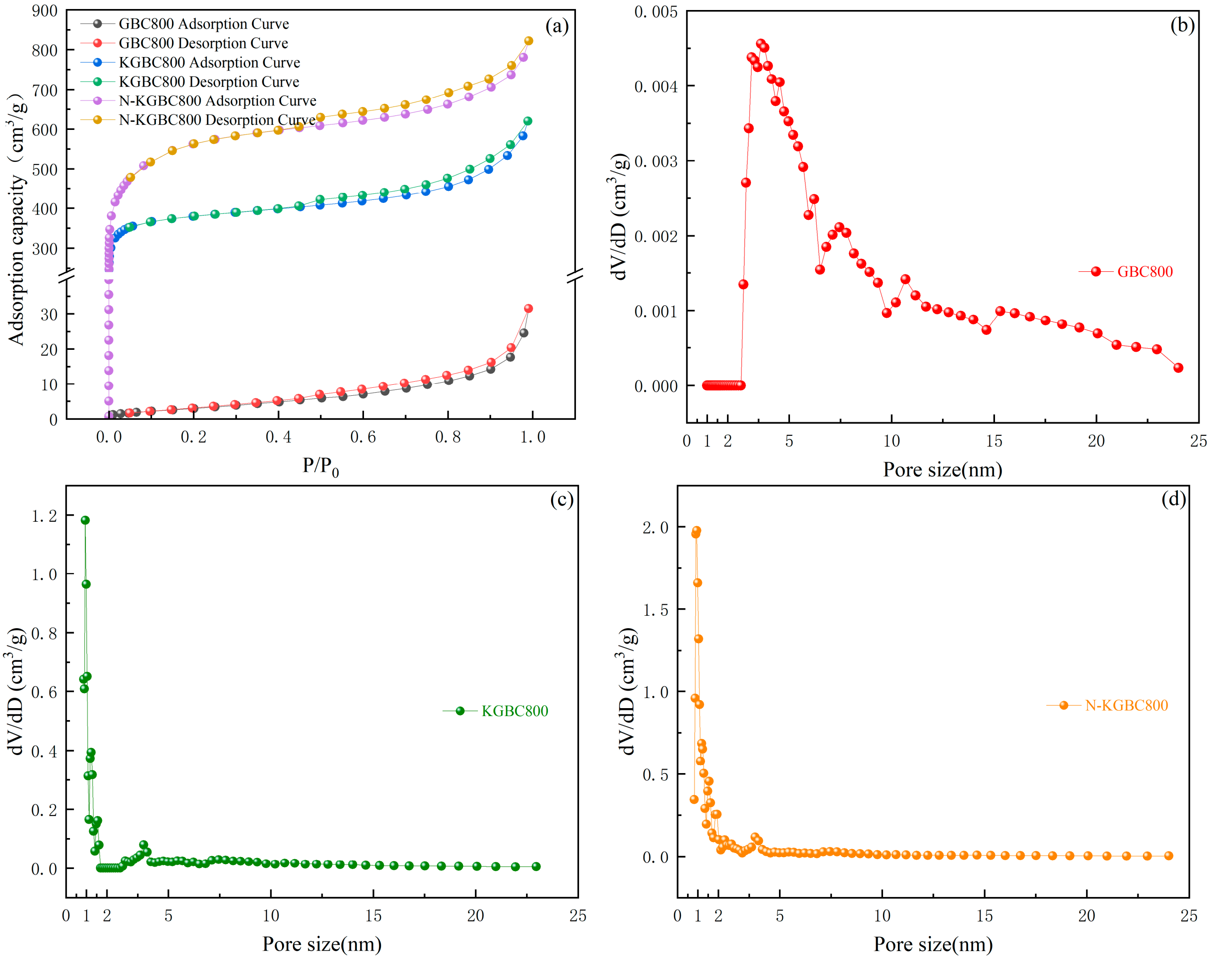

Figure 4. N_2 adsorption–desorption curves and pore size distribution curves of modified rape straw biochar. (**a**) Biochar N_2 adsorption–desorption curve; (**b**) GBC800 pore size distribution graph; (**c**) KGBC800 pore size distribution graph; and (**d**) N-KGBC800 pore size distribution graph.

Table 1. Modified rape straw biochar BET parameters.

Parameters	Unit	GBC800	KGBC800	N-KGBC800
S_{BET}	m^2/g	11.7	1477	2090
V_{Total}	cm^3/g	0.05	0.96	1.27
V_{Mic}	cm^3/g	0.00	0.41	0.36
L_0 [1]	nm	16.56	2.59	2.43

Note: [1] The average pore size.

The pore structure of biochar is mainly divided into three types: macropore with a pore radius greater than 50 nm, micropore with a pore radius less than 2 nm, and mesoporous with a pore radius between 2–50 nm. According to IUPAC [29], GBC800, KGBC800 and N-KGBC800 belong to type IV adsorption isotherms. A significant hysteresis loop can be observed at $p/p_0 > 0.4$, which is due to capillary condensation occurring in mesoporous materials, indicating the presence of mesoporous biochar [30]. By observing (a) in Figure 4, it is found that GBC800 has no obvious inflection point at $p/p_0 < 0.1$, indicating that there are a large number of mesoporous pores on the surface of GBC800, while the number of micropores is very small, which is consistent with the aperture distribution diagram. However, KGBC800 and N-KGBC800 have steep turning points before $p/p_0 < 0.1$, indicating that they contain abundant micropore structures. Combined with (c,d) in Figure 4, it can be seen that micropores occupy a dominant position in their structures. However, according to parameter V_{mic} in Table 1, the micropore volume of KGBC800 accounts for 42.64% of the total pore volume. The micropore volume of N-KGBC800 accounted for 28.61% of the total pore volume, because the number of micropores on the biochar surface did not necessarily have a positive correlation with V_{Mic}/V_{Total}. Although the average pore widths of KGBC800 and N-KGBC800 are 2.59 nm and 2.43 nm, respectively, the presence of a large number of micropores on the surface still indicates that they belong to microporous materials.

3.1.2. Analysis of Chemical Properties of Materials

FT-IR was used to characterize and analyze the functional groups on the surface of biochar, and the characterization results are shown in Figure 5. In the figure, The main characteristic peaks of GBC800, KGBC800, and N-KGBC800 appeared around 3425 cm^{-1}, 2918 cm^{-1}, 2850 cm^{-1}, 1618 cm^{-1}, and 1094 cm^{-1}. However, it is worth noting that a new characteristic stretching peak appears near 1386 cm^{-1} for N-KGBC800. The stretching peak near 3425 cm^{-1} can be attributed to the O–H stretching of phenols, alcohols, and water molecules [31]. Furthermore, the peak intensities of GBC800 and N-KGBC800 are significantly greater than that of KGBC800, which may be related to the N–H bond therein. The stretching peak near 2918 cm^{-1} is produced by the asymmetric stretching vibration of alkyl–CH_2 or the contraction vibration of C–H [32]. The stretching peak near 2850 cm^{-1} is in line with the symmetrical stretching vibration of alkyl–CH_2 [33]. The stretching peak near 1618 cm^{-1} is the C=C or C=O transformed from the aromatic ring in the biomass lignocellulose [34]. N-KGBC800 and GBC800 have a weak absorption peak at 1386 cm^{-1}, mainly due to the C–N single bond formed by the affinity addition reaction between the external nitrogen source or the internal nitrogen source of the biomass and the hydroxyl and epoxy compounds [35]. A wide absorption peak appears near 1094 cm^{-1}, which is the characteristic peak of the aliphatic C–N stretching vibration [16]. The absorption peak of GBC800 at 799 cm^{-1} is caused by the out-of-plane deformation vibration of the aromatic C–H, and the absorption peak near 462 cm^{-1} is the stretching vibration of the Si–O–Si bond of the inorganic salt component [36].

The absorption peaks of the three kinds of biochar at 3425 cm^{-1} were obviously broad and strong; this is the telescopic oscillation of free or bonded –OH on carboxyl, hydroxyl, and carbonyl groups, and the presence of –OH is favorable for the occurrence of ion-exchange adsorption [37]. Zhao Xingchain et al. [38] showed that the intensity of the –OH absorption peak decreases and stabilizes with an increasing pyrolysis temperature, which indicates that the combined water is detached and the hydrogen-bonded hydroxyl group is broken. The magnitude of intensity at 1618 cm^{-1} was in the order of N-KGBC800 > KGBC800 > GBC800, suggesting that the aromatization of biochar was enhanced due to the increase in thermolysis and the introduction of $KHCO_3$. In contrast, the introduction of doped nitrogen intensified the aromatization. A smaller peak at 1386 cm^{-1} for N-KGBC800 indicates that there are still many reactive –NH_2 functional groups on its surface [35]. The absorption intensity at 1090 cm^{-1} (C–N) was GBC800 > N-KGBC800 > KGBC800, indicating that the number of nitrogen-containing functional groups in the biochar decreases due to the activation effect of $KHCO_3$ and then increases with the doping of urea, directly proving that nitrogen element has been successfully doped into the modified biochar, which is a direct proof of the successful doping of nitrogen into the modified biochar [21].

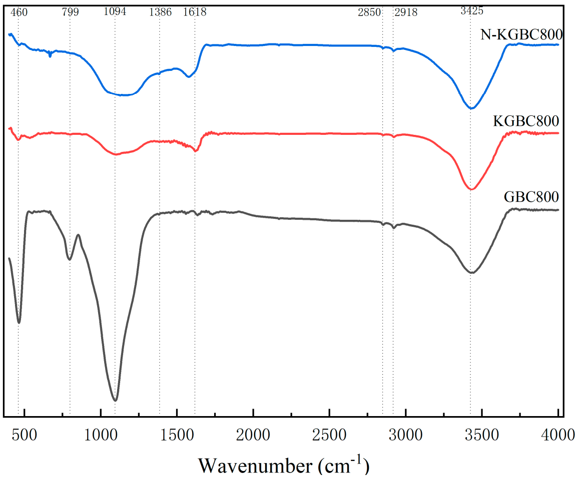

Figure 5. FT-IR plots of different biochar materials.

As can be seen from the proportion of elements on the surface of biochar in Table 2, the elements that make up the surface of biochar are mainly C and O. All the absorption peaks of the three biochars are at the same position. However, the intensities are inconsistent, indicating that the functional groups between GBC800, KGBC800, and N-KGBC800 are similar. According to the results in Figure 6, the obvious O1s peak (523.08 eV), the C1s peak (284.80 eV), and the weaker N1s peak (400.08 eV) can be observed. After the activation and nitrogen doping of the biochar, the O1s peak is significantly lower than that of the unmodified biochar, while the intensity of the C1s peak increases, indicating that after activation by $KHCO_3$, the oxygen-containing functional groups decrease and the degree of carbonization is higher. From the perspective of the elemental composition on the surface of the biochar, the N content of the unmodified biochar is relatively high. However, N decreases sharply after activation, while N doping by urea compensates for the loss of nitrogen-containing functional groups caused by high temperature to a certain extent [21].

Table 2. The elemental composition of different biochar surfaces.

Biochar	**Percentage of Surface Elements/%**			
	O1s	**C1s**	**N1s**	**Other Elements**
GBC800	25.22	63.41	1.15	10.22
KGBC800	13.82	84.32	0.45	1.41
N-KGBC800	13.37	83.95	1.04	1.64

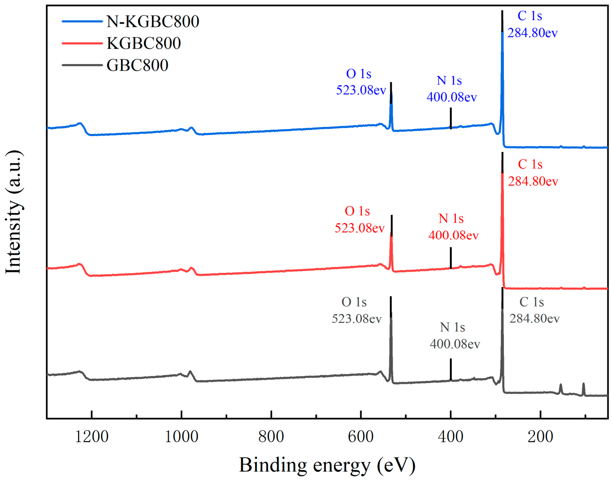

Figure 6. The XPS spectra of different biochar materials.

3.2. Effect of pH on the Performance of Biochar for TC Adsorption

The general solution pH of tetracycline is about 3.5, and the adsorption effect of TC with an initial pH in the range of 3~11 was investigated in this experiment. The biochar dosage was 0.15 g/L, the concentration of TC was 100 mg/L, the reaction temperature was 25 °C, and the reaction time was 12 h. The results of the adsorption process are presented in Figure 7.

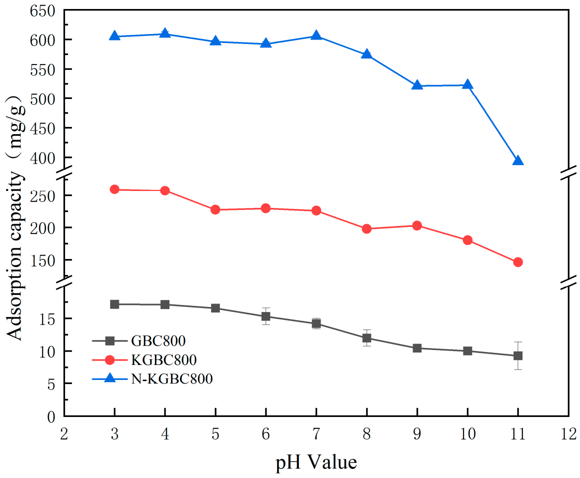

Figure 7. The effect of the pH on the impact of TC adsorption by biochar.

TC is a hydrophilic amphoteric substance, the p_{Ka1}, p_{Ka2}, and p_{Ka3} of which are 3.3, 7.7, and 9.7, respectively. Under different pH conditions, the existing forms of TC are different. When the $pH < 3.4$, it is mainly TC^+; when $3.4 < pH < 7.6$, it is mainly TC^0; when $7.6 < pH < 9.7$, it is mainly TC^-; and when the $pH > 9.7$, it is mainly TC^- and TC^{2-}. Biochar has a zero-charge point (pH_{pzc}). When the pH of the solution $< pH_{pzc}$, the biochar surface is mainly positively charged, and vice versa, it is negatively charged [39].

With an increase in the solution pH, the adsorption of the TC on three biochars showed approximately the same trend, with the maximum adsorption around pH = 3 and then a gradually decreasing trend, consistent with the study by Xiang et al. [40]. The maximum equilibrium adsorption capacities of TC by GBC800, KGBC800, and N-KGBC800 are 16.73 mg/g, 259.33 mg/g, and 609.06 mg/g, respectively. At this time, the protonation degree of the surface functional groups of biochar is relatively high, and TC also exists in the form of TC^+ or TC^0 [41]. The adsorption capacity should be weak, but the experimental results show the maximum adsorption capacity. This indicates that electrostatic interaction is not the main factor affecting the adsorption process at this time. When the pH is 4–5 and 7–9, all three kinds of biochar show a certain degree of decline. This is because as the pH increases, the surface of the biochar has negative charges, and TC also exists in the form of TC^0 ($3.4 < pH < 7.6$), TC^- ($7.6 < pH < 9.7$), and TC^{2-} ($pH > 9.7$) in the solution. The electrostatic repulsion between biochar and TC increases, resulting in a significant decrease in adsorption capacity. When the $pH > 9$, the strong repulsion between negatively charged biochar and TC^-, TC^{2-} makes the adsorption more difficult, resulting in a lower adsorption efficiency of TC. When there is a chemical adsorption process in the adsorption system, when the alkalinity is too strong, the active sites on the surface of the biochar will be passivated, thereby causing a sharp decline in the adsorption capacity of the biochar [42].

3.3. Influence of Biochar Dosage on TC Adsorption Performance

The dosage of the three kinds of biochar (GBC800, KGBC800, and N-KGBC800) was 0.05, 0.10, 0.15, 0.20, 0.25, 0.30, 0.35, and 0.40 g/L, respectively; the concentration of TC was 100 mg/L; pH ≈ 3.5; the reaction temperature was 25 °C; the reaction time was 60 min; and the oscillation frequency was 150 r/min. The experimental results are shown in Figure 8.

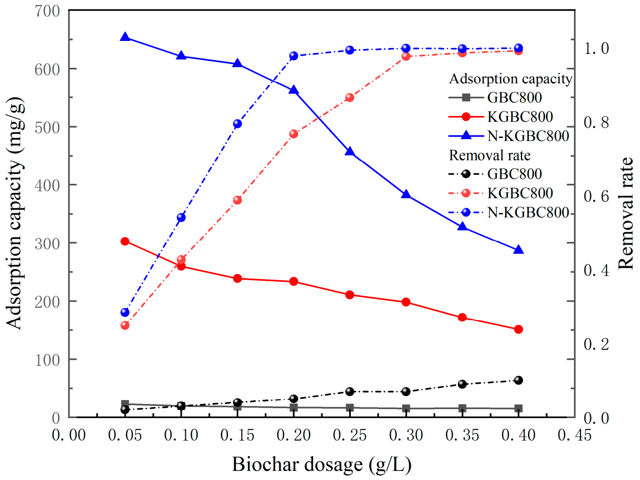

Figure 8. The influence of the biochar dosage on TC-adsorption effects.

An increase in the biochar dosage from 0.05 g/L to 0.4 g/L reduced the adsorption of TC by GBC800, KGBC800, and N-KGBC800, with a corresponding decrease from 21.4 to 14.98 mg/g. The adsorption of TC by GBC800, KGBC800, and N-KGBC800 decreased from 21.4 mg/g to 14.98 mg/g, 302.5 mg/g to 151.0 mg/L, and 652.8 mg/L to 286.8 mg/L, respectively; meanwhile, the removal rate increased from 2% to 10%, 24.7% to 99.05%, and 28.3% to 99.76%, respectively. The dosage of biochar showed a positive correlation with the TC removal rate within a certain range, while it showed a negative correlation with the adsorption amount. Deng Yu et al. [43] also indicated that the TC removal rate gradually increased with biochar addition. In contrast, the adsorption amount showed the opposite trend when preparing corn cob biochar for tetracycline adsorption. The primary rationale for this phenomenon is that an elevated dose of biochar can augment the number of functional groups and the number of efficacious active sites engaged in adsorption, which greatly enhances the possibility of contact between the biochar and TC in solution, resulting in almost close to 100% removal of TC in the solution [44]. In order to ensure the removal effect of TC, the best dosage of KGBC800 is about 0.25~0.3 g/L, and the best dosage of N-KGBC800 is about 0.15~0.2 g/L.

3.4. Adsorption Kinetic Modeling Analysis

Under the conditions of a TC concentration of 10, 50, and 100 mg/L; dosage of adsorbent of 0.15 mg/L; temperature of reaction of 25 °C; and adsorption duration of

720 min, the effects of TC adsorption by modified biochar were studied and kinetically analyzed based on the experimental data of this phase. Three types of kinetics, quasi-primary, quasi-secondary, and Elovich, and the model of intra-particle diffusion (the following equation), have been used to fit the relevant experimental data [45–47]. The kinetic fitting results are shown in Figure 9, with data points and coefficients in Table 3.

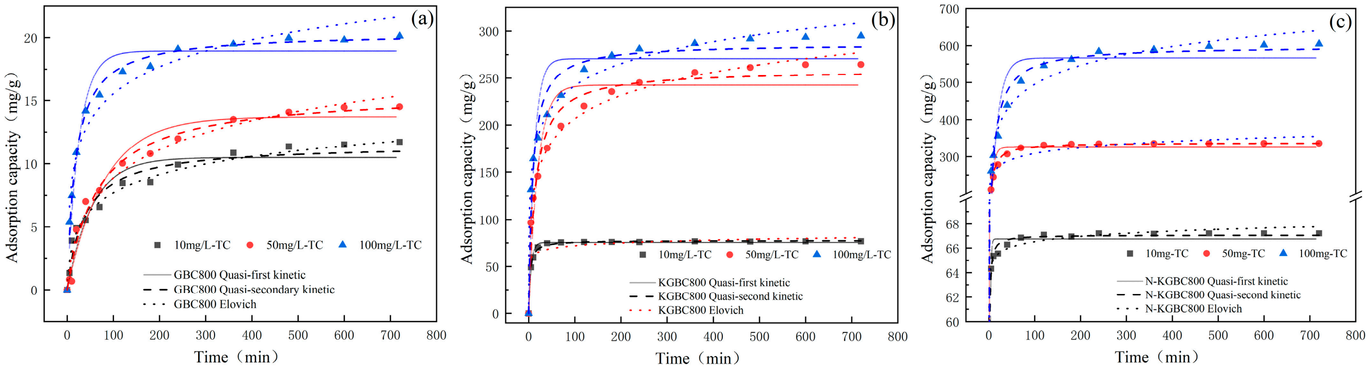

Figure 9. The adsorption kinetics model of TC adsorption by biochar: (**a**) GBC800, (**b**) KGBC800, and (**c**) N-KGBC800.

Table 3. The estimation of kinetic model parameters for TC adsorption on biochar.

Biochar	Kinetic Model	Parameters	Initial TC Concentration		
			10 mg/L	50 mg/L	100 mg/L
GBC800	Quasi-primary kinetic model	K_1/min^{-1}	0.0186	0.0124	0.0383
		$q_{e1,exp}/(\text{mg}\cdot\text{g}^{-1})$	11.3514	14.0823	16.9700
		$q_{e1}/(\text{mg}\cdot\text{g}^{-1})$	10.4794	13.7089	17.9445
		R^2	0.9156	0.9643	0.8851
	Quasi-secondary kinetic model	K_2/min^{-1}	0.0023	0.0009	0.0026
		$q_{e2,exp}/(\text{mg}\cdot\text{g}^{-1})$	11.3514	14.0823	16.9700
		$q_{e2}/(\text{mg}\cdot\text{g}^{-1})$	11.5208	15.6983	18.4010
		R^2	0.9624	0.9836	0.9399
	Elovich kinetic model	$\beta(\text{mg/g})$	0.4773	0.2928	0.3214
		R^2	0.9276	0.9568	0.9345
KGBC800	Quasi-primary kinetic model	K_1/min^{-1}	0.1830	0.0503	0.0799
		$q_{e1,exp}/(\text{mg}\cdot\text{g}^{-1})$	76.5766	264.4726	294.8649
		$q_{e1}/(\text{mg}\cdot\text{g}^{-1})$	75.4745	242.3914	270.7169
		R^2	0.9909	0.9002	0.8927
	Quasi-secondary kinetic model	K_2/min^{-1}	0.0046	0.0002	0.0004
		$q_{e2,exp}/(\text{mg}\cdot\text{g}^{-1})$	76.5766	264.2799	294.8469
		$q_{e2}/(\text{mg}\cdot\text{g}^{-1})$	77.4602	258.8755	286.5655
		R^2	0.9974	0.9700	0.9674
	Elovich kinetic model	$\beta(\text{mg/g})$	0.2281	0.0279	0.02954
		R^2	0.9529	0.9636	0.9508
N-KGBC800	Quasi-primary kinetic model	K_1/min^{-1}	0.6549	0.16286	0.063
		$q_{e1,exp}/(\text{mg}\cdot\text{g}^{-1})$	67.2072	336.0661	604.7147
		$q_{e1}/(\text{mg}\cdot\text{g}^{-1})$	66.7497	326.7898	566.6394
		R^2	0.9987	0.9665	0.9166
	Quasi-secondary kinetic model	K_2/min^{-1}	0.0624	0.0008	0.0001
		$q_{e2,exp}/(\text{mg}\cdot\text{g}^{-1})$	67.2072	336.0661	604.7147
		$q_{e2}/(\text{mg}\cdot\text{g}^{-1})$	67.0695	337.5815	598.7235
		R^2	0.9997	0.9969	0.9772
	Elovich kinetic model	$\beta(\text{mg/g})$	1.5842	0.0427	0.0135
		R^2	0.9796	0.9693	0.9804

Quasi-primary kinetic model:

$$\frac{dq_t}{d_t} = K_1(q_e - q_t) \tag{2}$$

Quasi-secondary kinetic model:

$$q_t = \frac{k_2 t q_e^2}{1 + k_2 t q_e} \tag{3}$$

Elovich kinetic model:

$$q_t = a + b \ln t \tag{4}$$

Intra-particle diffusion model:

$$q_t = K_{ip} t^{0.5} + C \tag{5}$$

q_e—The adsorbed amount of the adsorbent at equilibrium, mg/g.
q_t—The adsorbed amount of the adsorbent at time t, mg/g.
K_1—The quasi-primary kinetic adsorption rate constant, min^{-1}.
t—The adsorption time, min; K_2, the quasi-secondary kinetic modeling rate constant, g/(mg·min).
α—The initial adsorption rate, mg/(g·min).
b—The desorption constant.
K_{ip}—The intra-particle diffusion rate constant, and C is a constant.

As shown in Figure 9, given the fitting situation and the relevant fitting parameters in Table 3, the correlation coefficients R^2 of the quasi-secondary kinetic models for the three biosorption TCs at different initial concentrations were closer to 1. Furthermore, the average difference values between the theoretical saturated adsorption capacity q_{e1} obtained by the quasi-first-order kinetics simulation and the experimentally obtained saturated adsorption capacity $q_{e1,exp}$ for GBC800, KGBC800, and N-KGBC800 are −0.97 mg/g, 15.77 mg/g, and 47.80 mg/g, respectively. The average difference values between the theoretical saturated adsorption capacity q_{e2} obtained by the quasi-second-order kinetics simulation and the experimentally obtained saturated adsorption capacity $q_{e2,exp}$ are −0.43 mg/g, 3.30 mg/g, and 1.537 mg/g, respectively. This indicates that the fitting effect of the quasi-second-order kinetics is better than that of the quasi-first-order kinetics and the Elovich model. When the initial concentration of TC is 100 mg/L, the experimental saturated adsorption capacity of N-KGBC800 on TC is 604.71 mg/g, which shows the excellent adsorption capacity of the former compared with the saturated adsorption capacity of GBC800 16.97 mg/g. Although the overall nitrogen content on the surface of N-KGBC800 is slightly lower than that of GBC800, nitrogenous compound are slightly introduced to the surface of the biochar during the reaction process, and the newly introduced nitrogen-containing functional groups can increase the adsorption capacity, which is consistent with the study by Guo et al. [48]. This phenomenon may be attributed to the promotion of a reaction between nitrogen and oxygen groups on the surface of the biochar, which in turn facilitates the mutual transformation of nitrogen-containing functional groups [49]. The incorporation of nitrogen-containing functional groups diminishes the electronegativity of the C-layer, thereby enhancing its capacity to accept π-electrons and facilitating the formation of π–π bonds and Lewis acid–base interactions with organic molecules during adsorption. This ultimately results in an improvement in the adsorption capacity [50]. During the adsorption process, the uptake of TC by GBC800, KGBC800, and N-KGBC800 was the consequence of a synergistic interaction between physical and chemical adsorption. The chemical adsorption process was identified as the primary rate control step in this process. The adsorption process may be characterized by the sharing of electrons, the formation of valence bonds through electron exchange, and π–π interactions.

In order to gain further insight into the stages of the adsorption process, it is necessary to employ the intra-particle diffusion model for further analysis, and the model parameters are shown in Table 4. As illustrated in Figure 10, the adsorption process of TC by GBC800, KGBC800, and N-KGBC800 can be delineated into three linear phases. The initial stage is the outward transfer of TC molecules from the solution to the surface of the biochar. The second phase is the diffusion of these molecules from the surface into the internal pores. The subsequent phase is the equilibrium stage, during which chemical interactions occur between the TC molecules and the adsorption sites on the biochar. The model-fitting results indicate that the fitted curve of the intra-particle diffusion model consists of three linear cross-sections, which suggests that the adsorption rate is influenced by intra-particle diffusion. However, this does not represent the sole rate-controlling step, as other mechanisms, including liquid film diffusion, electrostatic interactions, hydrogen bonding, and interactions, are also involved in controlling the adsorption rate [49,51]. Given the constants C in Table 5, it can be observed that $C_{i,3} > C_{i,2} > C_{i,1}$ exists in all three steps, suggesting that liquid film diffusion may also be an influencing factor limiting the adsorption rate [52]. Prior to reaching adsorption equilibrium, TC molecules are transported from the solution to the surface of the biochar. This occurs initially via external mass transfer and liquid film diffusion, and subsequently, the molecules enter the inner pore structure and undergo adsorption on the internal surface of the biochar, a process that is controlled by intraparticle diffusion [39,53,54].

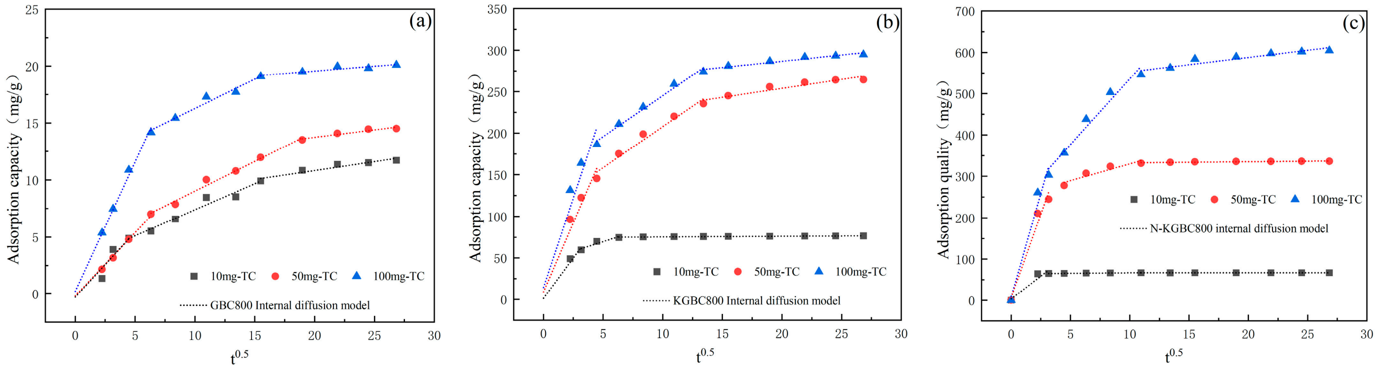

Figure 10. The intraparticle diffusion model of TC adsorption by biochar: (**a**) GBC800, (**b**) KGBC800, and (**c**) N-KGBC800.

Table 4. The parameter estimation of the internal diffusion model for TC adsorption by biochar.

Biochar	Parameters	Initial TC Concentration		
		10 mg/L	50 mg/L	100 mg/L
GBC800	$K_{GBC,1}$ [mg/(g·min)]	1.1472	1.1146	2.2700
	$C_{GBC,1}$ (mg/g)	−0.2934	−0.1857	0.2270
	$R_1{}^2$	0.8761	0.9948	0.9946
	$K_{GBC,2}$ [mg/(g·min)]	0.4552	0.5209	0.5179
	$C_{GBC,2}$ (mg/g)	2.8389	3.8104	11.0938
	$R_2{}^2$	0.9588	0.9835	0.9625
	$K_{GBC,3}$ [mg/(g·min)]	0.1546	0.1309	0.0856
	$C_{GBC,3}$ (mg/g)	7.7316	11.1160	17.8559
	$R_3{}^2$	0.8967	0.8797	0.8352

Table 4. *Cont.*

Biochar	Parameters	Initial TC Concentration		
		10 mg/L	**50 mg/L**	**100 mg/L**
KGBC800	$K_{\text{KGBC},1}$ [mg/(g·min)]	19.4498	33.3154	42.9313
	$C_{\text{KGBC},1}$ (mg/g)	1.2772	8.9329	14.5346
	$R_1{}^2$	0.9702	0.9425	0.9098
	$K_{\text{KGBC},2}$ [mg/(g·min)]	4.5743	9.8530	9.8794
	$C_{\text{KGBC},2}$ (mg/g)	46.8038	109.2741	146.3773
	$R_2{}^2$	0.8133	0.9556	0.9805
	$K_{\text{KGBC},3}$ [mg/(g·min)]	0.0784	2.1578	1.5079
	$C_{\text{KGBC},3}$ (mg/g)	74.5739	210.8439	256.5668
	$R_3{}^2$	0.8758	0.8816	0.9202
N-KGBC800	$K_{\text{N-KGBC},1}$ [mg/(g·min)]	22.1605	80.5541	99.6993
	$C_{\text{N-KGBC},1}$ (mg/g)	3.3464	6.9789	8.5941
	$R_1{}^2$	0.8522	0.9488	0.9493
	$K_{\text{N-KGBC},2}$ [mg/(g·min)]	0.2413	8.0325	31.8177
	$C_{\text{N-KGBC},2}$ (mg/g)	64.6160	249.5722	217.5784
	$R_2{}^2$	0.9359	0.8337	0.9533
	$K_{\text{N-KGBC},3}$ [mg/(g·min)]	0.0132	0.2524	3.4903
	$C_{\text{N-KGBC},3}$ (mg/g)	66.8827	329.9344	517.9382
	$R_3{}^2$	0.8348	0.8519	0.8541

Table 5. The estimation of isothermal parameters for TC adsorption by biochar.

Biochar	Model	Parameters	Reaction Temperature (T)		
			288 K	**298 K**	**308 K**
GBC800	Langmuir	q_m (mg/g)	16.1679	20.8750	24.1704
		K_L (L/mg)	1.0074	0.6959	0.3604
		R_L	0.0098	0.0141	0.0269
		R^2	0.9384	0.9220	0.9425
	Freundlich	K_F [mg·g^{-1}·(L·mg)$^{-1/n}$]	9.4458	10.2429	10.1680
		$1/n$	0.1476	0.1733	0.2011
		R^2	0.9235	0.9197	0.8894
	Temkin	b_T (kJ/mol)	1.2296	0.9503	0.7765
		K_T (L/mg)	90.1630	38.0677	15.2946
		R^2	0.9250	0.9768	0.9371
KGBC800	Langmuir	q_m (mg/g)	268.4533	285.3526	306.5144
		K_L (L/mg)	1.2706	1.4866	1.3825
		R_L	0.0078	0.0066	0.0071
		R^2	0.9886	0.9727	0.9823
	Freundlich	K_F [mg·g^{-1}·(L·mg)$^{-1/n}$]	149.3361	158.7649	167.5674
		$1/n$	0.1638	0.1691	0.1739
		R^2	0.8550	0.8649	0.8711
	Temkin	b_T (kJ/mol)	0.0717	0.0680	0.0648
		K_T (L/mg)	69.5907	65.3959	60.3399
		R^2	0.9377	0.9456	0.9523
N-KGBC800	Langmuir	q_m (mg/g)	630.5727	660.6366	688.3172
		K_L (L/mg)	1.0369	0.6756	0.6062
		R_L	0.0095	0.0145	0.0162
		R^2	0.9973	0.9917	0.9868
	Freundlich	K_F [mg·g^{-1}·(L·mg)$^{-1/n}$]	301.1075	300.6277	302.3327
		$1/n$	0.1987	0.2198	0.2306
		R^2	0.8163	0.8801	0.8787
	Temkin	b_T (kJ/mol)	0.0262	0.0261	0.0253
		K_T (L/mg)	25.6450	22.1160	18.4779
		R^2	0.9219	0.9549	0.9534

3.5. Adsorption Isotherm Modeling Analysis

The experimental data of TC adsorption in the solution for GBC800, KGBC800, and N-KGBC800 were isothermally fitted using the Langmuir model, Freundlich model, and Temkin model (as follows) in turn at temperatures of 288 K, 298 K, and 308 K, with a biochar dosage of 0. 15 mg/L and an adsorption time of 720 min. The isothermal adsorption fitting curves are shown in Figure 11, and the fitting parameters are shown in Table 5.

The Langmuir isothermal adsorption model:

$$\frac{C_e}{q_e} = \frac{C_e}{q_m} + \frac{1}{q_m K_L} \tag{6}$$

Freundlich isothermal adsorption model:

$$q_e = k_f \times C_e^{\frac{1}{n}} \tag{7}$$

The Temkin isothermal adsorption model:

$$q_m = \frac{RT}{b_T} \ln K_T + \frac{RT}{b_T} \ln C_e \tag{8}$$

q_e—The adsorption capacity of the adsorbent at the adsorption equilibrium, mg/g.
q_m—The theoretical saturated adsorption capacity of the adsorbent for pollutants, mg/g.
C_e—The pollutant concentration in the solution at the adsorption equilibrium, mg/L.
K_L—The Langmuir adsorption constant, L/mg, indicating the adsorption strength of the adsorbent for the adsorbate.
K_f—The Freundlich adsorption constant, (mg/g)·(L/mg)$^{1/n}$, indicating the adsorption capacity of the adsorbent, which is related to the properties and dosage of the adsorbent and the reaction temperature.
n—The nonlinear adsorption index, reflecting the heterogeneity of the adsorption sites on the surface of the adsorbent.
b_T and K_T are the constants of the Temkin model; R is the universal gas constant, J/(mol·K); and T is the Kelvin temperature, K.

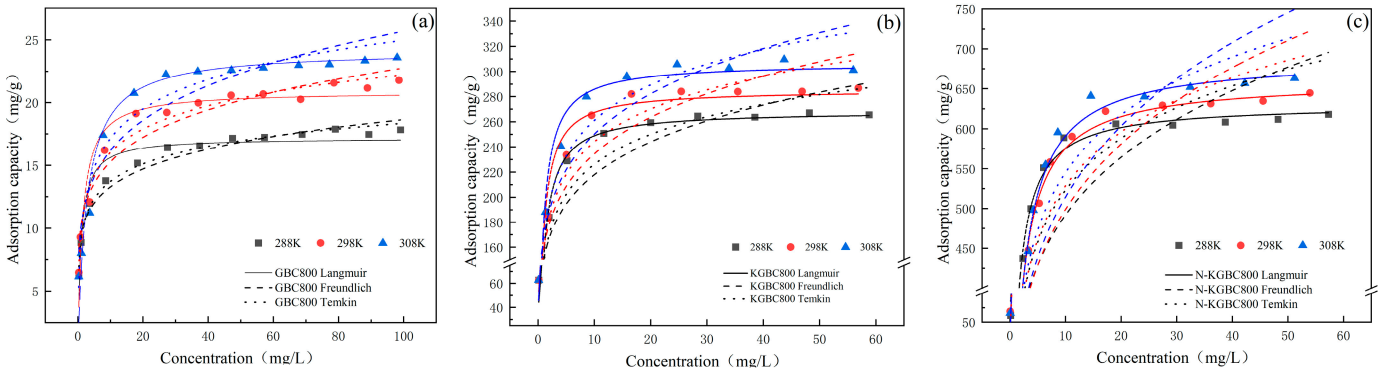

Figure 11. The isothermal modeling of TC adsorption by biochar: (**a**) GBC800, (**b**) KGBC800, and (**c**) N-KGBC800.

The fitting results indicate that the process of TC adsorption by GBC800, KGBC800, and N-KGBC800 at different temperatures is best described by the Langmuir model, followed by the Temkin and Freundlich models. This suggests that the adsorption process is biased toward monolayer adsorption, whereby a homogeneous monolayer of TC molecules is formed on the surface of the biochar, with chemical adsorption dominating the process [55]. The adsorption reaction is a process whereby the adsorbate continuously migrates from the main body of the aqueous phase to the solid adsorbent phase. In contrast, the concentration gradient between the two phases provides the main driving force for this migration. The adsorbent surface is energetically homogeneous; the adsorption sites are equipotent, there is no interaction between TC molecules, and the final equilibrium state of the adsorption is dynamic [56]. The fitting results of the Langmuir isothermal model indicate that the theoretical maximum adsorption capacities of GBC800, KGBC800, and N-KGBC800 at 25 °C are 16.16 mg/g, 268.45 mg/g, and 630.57 mg/g, respectively. The experimentally determined values are 16.82 mg/g, 265.48 mg/g, and 617.91 mg/g, respectively, which are basically consistent. This further confirms the applicability of the Langmuir model.

The correlation coefficient (R^2) of the Temkin isothermal model was found to be greater than 0.9 for all cases, indicating that the adsorption process of TC by GBC800, KGBC800, and N-KGBC800 was predominantly chemisorption-driven and that strong intermolecular forces played a pivotal role in the TC adsorption process [54]. b_T is an index of the reactive chemical interactions; the KGBC800 and N-KGBC800 b_T values are much lower than those of GBC800, indicating that the former two play a weaker role than the latter in the whole adsorption process by chemisorption [57]. This phenomenon may be attributed to the surface structure of GBC800 biochar. The lower specific surface area and less developed porosity of GBC800 result in a diminished role for physical adsorption in the TC-adsorption process. Consequently, the functional groups of the carbon surface become the primary means of contact between GBC800 and TC throughout the adsorption process.

3.6. Thermodynamic Analysis of Adsorption

A comprehensive analysis of the adsorption behavior of modified biochar on TC requires the thermodynamic characterization of the aforementioned process by the three biochars at three distinct temperatures: 298 K (25 °C), 308 K (35 °C), and 318 K (45 °C). The equations used are shown in (9)–(11), the fitting results are indicated by Figure 12, and the thermodynamic parameters are listed in Table 6.

$$\Delta G^{\theta} = -RT \times \ln k \tag{9}$$

$$\ln k = \frac{\Delta S^{\theta}}{R} - \frac{\Delta H^{\theta}}{RT} \tag{10}$$

$$\Delta G^{\theta} = \Delta H^{\theta} - T\Delta S^{\theta} \tag{11}$$

ΔG^{θ}—The Gibbs free energy, kJ/mol.
ΔH^{θ}—The enthalpy, kJ/mol.
ΔS^{θ}—The entropy, kJ/(mol·K).
T—The absolute temperature, K.
K—The Langmuir adsorption equilibrium constant, L/mg.
R—The universal gas constant, J/(mol·K), $R = 8.314 \times 10^{-3}$, KJ/(mol·K).

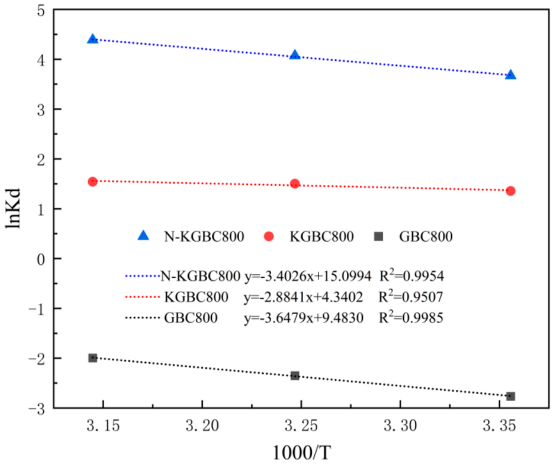

Figure 12. The thermodynamic modeling of TC adsorption on biochar.

Table 6. The estimation of thermodynamic parameters for TC adsorption on biochar.

Biochar	Parameters	Temperature (K)		
		298	**308**	**318**
GBC800	ΔG_0 (kJ/mol)	6.8480	6.0157	5.2736
	ΔH_0 (kJ/mol)		30.2920	
	ΔS_0 (J/mol·K)		0.0787	
	R^2		0.9989	
KGBC800	ΔG_0 (kJ/mol)	−3.3619	−3.8494	−4.0779
	ΔH_0 (kJ/mol)		27.2631	
	ΔS_0 (J/mol·K)		0.0358	
	R^2		0.9782	
N-KGBC800	ΔG_0 (kJ/mol)	−9.0964	−10.4260	−11.6034
	ΔH_0 (kJ/mol)		28.232	
	ΔS_0 (J/mol·K)		0.1253	
	R^2		0.9998	

The enthalpy changes (ΔH) of TC adsorption of GBC800, KGBC800, and N-KGBC800 were 30.2920 kJ/mol, 27.2631 kJ/mol, and 28.232 kJ/mol, respectively, and their enthalpy changes were positive, indicating that the adsorption process is a thermally active reaction and that it is more favorable for adsorption at higher temperatures. This is in agreement with the results of the adsorption isotherm fitting. In addition, according to the results of Garba et al. [58], the enthalpy change ΔH being lower than 20 kJ/mol adsorption is mainly a physical reaction. Vice versa, it is dominated by chemical action, and the adsorption behaviors of GBC800, KGBC800, and N-KGBC800 are all greater than 20 kJ/mol, indicating that the adsorption behaviors of all three to TC in water are heat-absorbing reactions and dominated by chemical adsorption. Significant adsorption between adsorbent and adsorbate can occur when the free energy of the adsorption ΔG value is negative [59]. The adsorption of TC on the surface of the adsorbent was observed to be spontaneous in all cases, and the absolute value of ΔH was found to increase with the rise in temperature. This indicates that the spontaneous tendency of the process of adsorption of TC by N-KGBC800 and KGBC800 increases with the rise in ambient temperature and that the temperature rise is beneficial for the adsorption process. The entropy changes (ΔS) of GBC800, KGBC800, and N-KGBC800 in the adsorption of TC were 0.0296 J/(mol·K), 0.0357 J/(mol·K), and 0.1008 J/(mol·K), respectively. These values indicate that the adsorption process was less reversible. The adsorption process can be described as a dynamic equilibrium between adsorption and desorption, with a positive adsorption value that is significantly higher than the desorption value [60]. Furthermore, as the adsorption process progresses, the solid–liquid interface disorder gradually increases, stabilizing the adsorption process.

3.7. Adsorption Mechanism Analysis

In order to better explore the adsorption mechanism of modified biochar on TC, the biochar after adsorption and adsorption saturation was placed in 0.05 mol/L NaOH solution for analysis for 3 h and rinsed with deionized water repeatedly until pH ≈ 7. After being desorbed, separated, and dried, the biochar was obtained. The BET and FT-IR characterization of the biochar were performed to compare the changes of pore structure and surface functional groups before and after the adsorption of TC by biochar.

As illustrated in Figure 13, the BET characterization of biochar following the adsorption of tetracycline yielded the following results. The number of micropores in the adsorbed biochar was significantly reduced, and there was no significant change in mesopores. When comparing Tables 1 and 7, the specific surface areas of GBC800, KGBC800, and N-KGBC800 after adsorption are 9.634 m^2/g, 1035.101 m^2/g, and 784.946 m^2/g, respectively, and the total pore volumes are 0.03658 cm^3/g, 0.8192 cm^3/g, and 0.6179 cm^3/g, respectively. Compared with before adsorption, the specific surface area of GBC800 decreased by 18.19%, and the total pore volume decreased by 12.67%; the specific surface area of KGBC800 decreased by 29.96%, and the total pore volume decreased by 14.58%; the specific surface area of N-KGBC800 decreased by 62.45%, and the total pore volume decreased by 51.42%. Kowalczyk et al. [61] proposed that carbon materials with pore diameters of approximately 1.4–1.6 nanometers may cause the molecular-sieving effect of TC. Therefore, the reduction in the surface area and pore volume of KGBC800 and N-KGBC800 mainly occurs when the pore diameter is smaller than the dynamic diameter of TC, which may be due to the blocking of pores by TC molecules. Generally speaking, pores larger than 1–2 times the diameter of the adsorbate molecule show good adsorption performance [25]. The dynamic diameter of TC molecules is approximately 1.27 nm, and the average pore diameters of GBC800 are 16.56 nm. Moreover, the BET and SEM of GBC800 characterization results show that its pores are poorly developed. Therefore, the adsorption capacity of GBC800 for TC is weak. The average pore diameters of KGBC800 and N-KGBC800 are 2.5956 nm and 2.4325 nm, respectively. Tetracycline molecules can easily enter the pore structures of the two biochars, and their microporous structures can be fully utilized as adsorption sites for tetracycline. Thus, one of the main mechanisms for the removal of tetracycline from water by modified biochar is pore-filling.

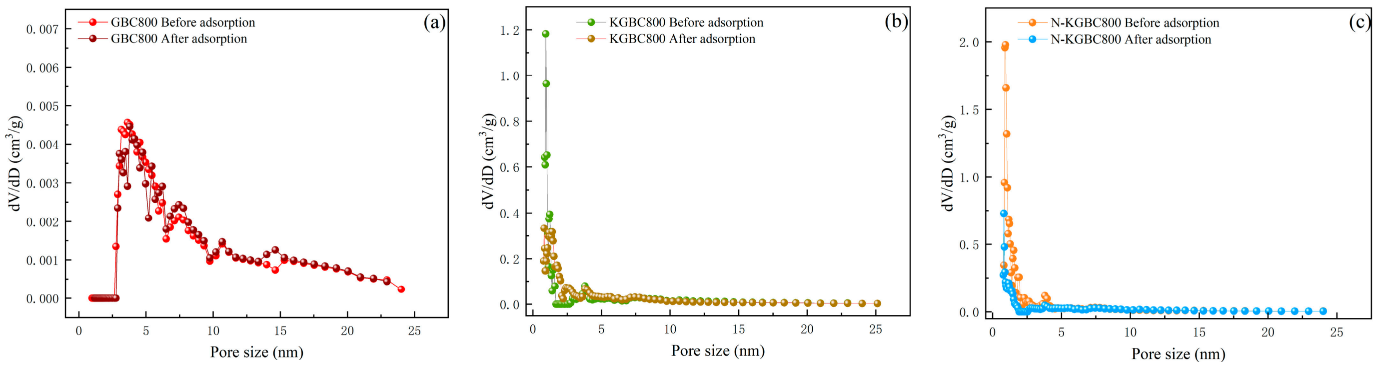

Figure 13. The distribution of front and rear absorption holes: (**a**) GBC800, (**b**) KGBC800, and (**c**) N-KGBC800.

Table 7. BET parameters after TC adsorption on biochar.

Parameters	Unit	GBC800	KGBC800	N-KGBC800
S_{BET}	m^2/g	9.6	1035	785
V_{Total}	cm^3/g	0.04	0.82	0.62
V_{Mic}	cm^3/g	0.00	0.17	0.19
L_0 [1]	nm	13.50	3.16	3.15

Note: [1] The average pore size.

Comparing the FT-IR patterns of GBC800, KGBC800, and N-KGBC800 before and after adsorption (Figure 14), the data demonstrate that the absorption peaks of all three types of biochars at approximately 3425 cm^{-1} are all shifted to the right and exhibit a reduction in peak intensity. This suggests that the oxygen-containing functional groups present in the biochar were involved in the adsorption reaction, potentially interacting with the hydroxyl, amino, carboxyl, and other functional groups on the TC molecule to form hydrogen bonds or n–π interactions. It is similarly conceivable that the nitrogen-containing functional groups on the surface of the biochar may have undergone a chemical bonding process with the TC, which could have resulted in a change in the position of its telescopic vibration [62–64]. The C=C and C=O (near 1618 cm^{-1}) absorption peaks of N-KGBC800 are significantly shifted, indicating that there may be a π–π stacking interaction between the aryl ring structure on N-KGBC800 and the TC [65]. At C-N (1094 cm^{-1}), the peak intensities before and after the adsorption of GBC800 and N-KGBC800 changed significantly, while

KGBC800 remained almost unchanged, which may be attributed to the Lewis acid–base interactions between nitrogen-containing functional groups on the surface of the biochar and the TC molecules. Furthermore, the amino group, which is formed by the deprotonation of tetracycline, can undergo a reaction with the benzene ring present in biochar, resulting in the formation of a cationic–π interaction [66]. When the solution pH is higher than the zero-point charge of biochar, the oxygen-containing functional groups on the surface of biochar undergo deprotonation, thereby acquiring a negative charge. This promotes the electrostatic interaction between biochar and tetracycline [67,68].

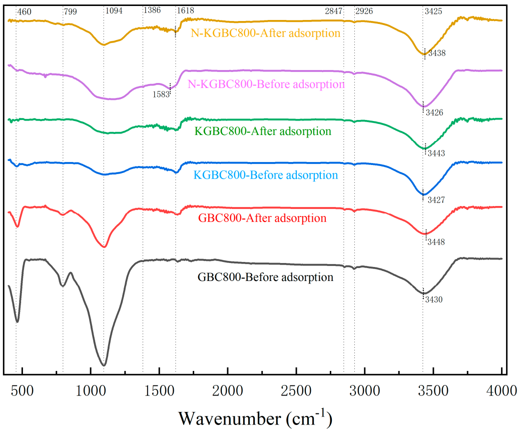

Figure 14. A comparison of FT-IR changes before and after TC adsorption on biochar.

Based on the above-mentioned discussion, the adsorption mechanisms of GBC800, KGBC800, and N-KGBC800 for TC in the adsorption are shown in Figure 15. The adsorption processes of the three biochars for TC are basically the same, and they are all the results of the combined effect of physical and chemical actions. The difference lies in the different intensities of different actions. Specifically, TC in the solution rapidly diffuses to the surface of the biochar, resulting in liquid film diffusion, and continuously fills the macropores, mesopores, and micropores of the biochar. The TC molecules entering the pores form electrostatic interactions with the charged groups on the surface of the biochar, interact with oxygen-containing functional groups such as –OH to form hydrogen bonds or *n*–π interactions, have Lewis acid–base interactions with nitrogen-containing functional groups, and form π–π stacking or cation–π interactions between the aromatic ring structure of the carbon itself and TC.

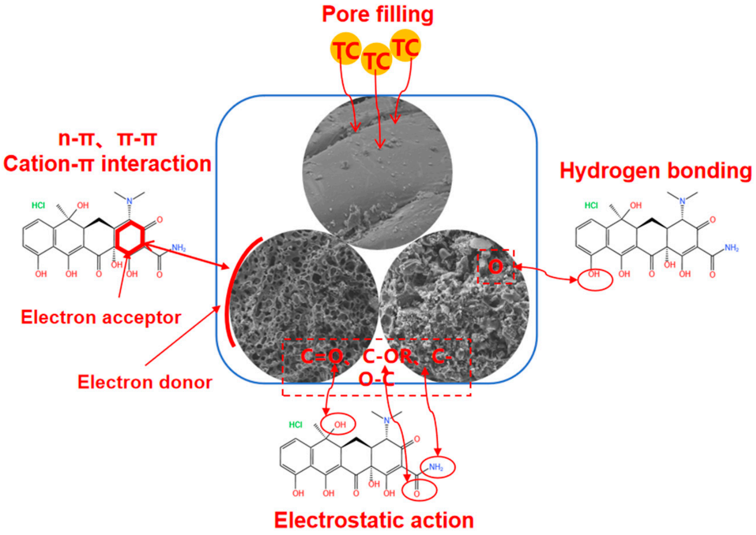

Figure 15. An adsorption mechanism diagram of TC adsorption on modified biochar.

3.8. Experimental Adsorption of Tetracycline on Biochar Fixed-Bed and Adsorption Model Analysis

After modification, the adsorption and removal effects of rapeseed straw biochar (KGBC800 and N-KGBC800) on TC in water were greatly improved compared to those of unmodified GBC800 of rapeseed straw, and they can effectively remove TC in water. Adsorption can be divided into batch and fixed-bed adsorption according to different operation modes. In practical applications, batch adsorption has many limitations, such as influent water, reaction site, operation management, etc. In the fixed-bed adsorption process, the length of the effective mass-transfer zone moves along the liquid flow to the entire bed depth until the fixed bed is fully utilized [69]. Compared with batch adsorption, the fixed-bed reactor is more economical, operable, and has a continuous processing capacity, thus becoming the mainstream wastewater treatment method. This chapter investigates the dynamic adsorption behaviors of three TC on biochars in pure water and salt water and uses the Thomas model and Yoon–Nelson mass-transfer model to conduct further analysis of dynamic adsorption.

3.8.1. Biochar Fixed-Bed Adsorption of Tetracycline Experiment

The penetration point in the dynamic adsorption process is defined as C_t/C_0 = 0.05, indicating that the TC effective concentration is approximately 5% of the initial concentration. The adsorption saturation point is C_t/C_0 = 0.95, representing an effective TC concentration of approximately 95% of the initial concentration. As shown in Figure 16, the penetration points of GBC800, KGBC800, and N-KGBC800 in the dynamic adsorption process under pure water conditions were 10 min (when the adsorption penetration point < 10 min, it was set as 10 min), 70 min, and 270 min, respectively, and the adsorption penetration points under brine conditions were 10 min, 40 min, and 240 min, respectively. As the adsorption sites of biochar in the adsorption column were gradually consumed, the concentration of TC in the effluent gradually increased and finally reached saturation. The saturation points of the dynamic adsorption process of GBC800, KGBC800, and N-KGBC800 were 60 min, 210 min, and 460 min in pure water, and the adsorption penetration points were 40 min, 190 min, and 270 min in brine, respectively. The adsorption penetration points under saline conditions were 40 min, 190 min, and 390 min, respectively.

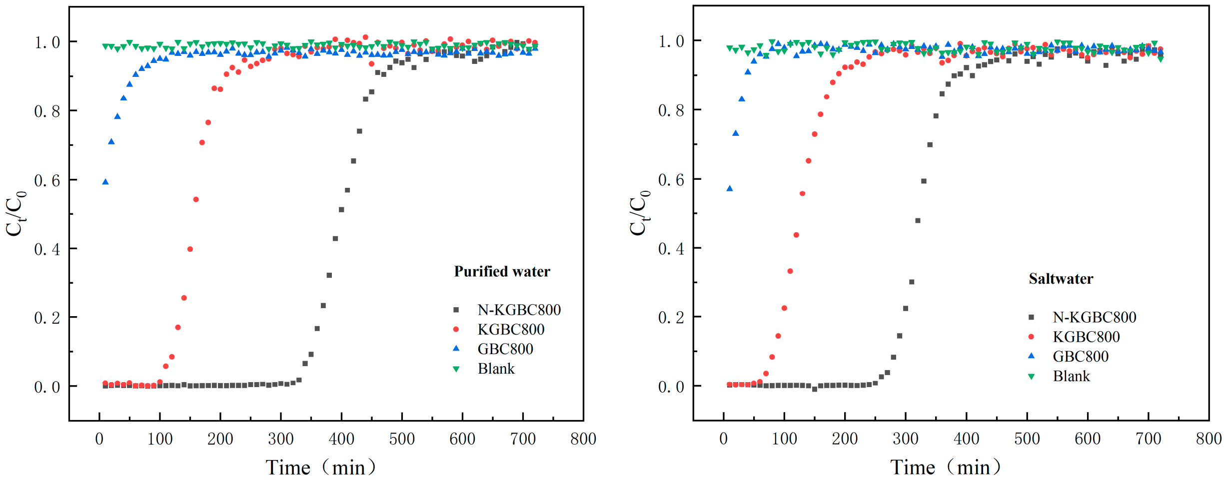

Figure 16. The adsorption effect of biochar fixed bed on TC under different conditions.

The adsorption properties of GBC800, KGBC800, and N-KGBC800 showed obvious differences in the process of dynamic adsorption of TC. The saturated adsorption capacities of GBC800, KGBC800, and N-KGBC800 were calculated by integral method and were 15.11 mg/g, 238.37 mg/g, and 601.03 mg/g, respectively, under pure water conditions. Under saline conditions, the results were 11.63 mg/g, 211.93 mg/g and 573.42 mg/g, respectively. A range of inorganic ions present in brine exert a discernible inhibitory effect on the adsorption performance of the fixed bed of biochar. Moreover, a considerable quantity of Na^+ in the solution has been found to exert a certain inhibitory effect on the adsorption of tetracycline. Furthermore, the adsorption of tetracycline can be significantly disrupted by the presence of Mg^{2+} and Ca^{2+}. The presence of an electrostatic effect between Ca^{2+} and the adsorbent of biochar, on the one hand, and the presence of Ca^{2+} with the adsorbent of biochar, on the other hand, results in competition between Ca^{2+} and TC for hydroxyl groups on the surface of biochar. This leads to a reduction in the number of adsorption sites on the surface of the adsorbent [70]. Zhao et al. [71] demonstrated that divalent cations exhibit higher ionic strengths, resulting in a greater salting-out effect in solution than the crowding-out effect. Additionally, the higher covalency of divalent cations reduces the number of adsorption sites available on the surface of the adsorbent, consequently leading to a decline in the adsorption capacity for TC. In contrast, the anions chloride (Cl^-) and sulfate ($SO_4{}^{2-}$) have been observed to exert a negligible effect on the TC-adsorption capacity of biochar [56].

3.8.2. Biochar Fixed-Bed Adsorption Modeling

The Thomas model is a descriptive and evaluative tool that can be used to analyze the penetration curve of pollutants in a fixed bed, as well as to assess the adsorption capacity of the adsorbent in relation to the pollutants. It can also be employed to estimate the equilibrium adsorption amount of the adsorbent and the adsorption rate constants [72–74]. The Yoon–Nelson adsorption model predicts the trend of the whole adsorption curve and fits the typical penetration curves with an S-shape very well, mainly predicting 50% of the penetration time. The pertinent curves are illustrated in Figure 17, and the pertinent data are enumerated in Table 8.

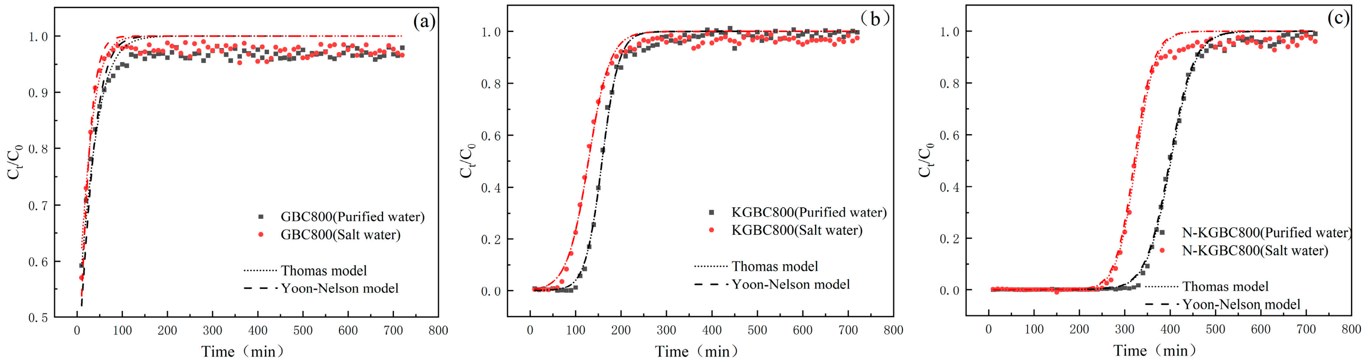

Figure 17. The fitting results of the Thomas model and Yoon–Nelson model. (**a**) GBC800, (**b**) KGBC800 and (**c**) N-KGBC800.

Table 8. The fitting parameters estimation of the Thomas model and the Yoon–Nelson model for the adsorption of TC by a biochar fixed bed.

Biochar	**Conditional**	**Thomas Model Parameters**				**Yoon–Nelson Model Parameters**		
		K_T (mL/(mg·min))	**q_e (mg/g)**	**q_{exp} (mg/g)**	**R^2**	**K_Y (L/min)**	**τ (min)**	**R^2**
GBC800	Purified water	0.3664	16.7136	15.1134	0.8842	0.0482	8.3346	0.8711
	Salted water	0.5024	15.4731	11.6302	0.8513	0.0716	7.8948	0.8321
KGBC800	Purified water	0.4325	262.0138	238.3792	0.9949	0.0424	158.2122	0.9872
	Salted water	0.5212	230.5852	211.9348	0.9897	0.0540	128.0997	0.9818
N-KGBC800	Purified water	0.3721	599.7145	601.0326	0.9973	0.0379	399.2547	0.9971
	Salted water	0.4690	585.2991	573.4281	0.9938	0.0479	321.3415	0.9932

The fitting coefficients R^2 for TC adsorption under pure water conditions were 0.8842, 0.9949, and 0.9973 for GBC800, KGBC800, and N-KGBC800, respectively, and 0.8513, 0.9897, and 0.9938 for the adsorption of TC under brine conditions, respectively, which shows that the Thomas model was better able to describe, to a certain extent, the fixed-bed adsorption process of TC by KGBC800 and N-KGBC800. At the same time, it is slightly less effective in describing GBC800. In the Thomas model, there is an inverse relationship between the magnitude of K_T obtained for the same adsorbent under different reaction conditions and the equilibrium adsorption amount q_e. In contrast, the K_T between different adsorbents reflects the strength of the adsorbent to the adsorbate per unit of time [75]. Observing the K_T values obtained from the fitting, K_T (pure water) < K_T (brine) existed for all three biochars, indicating that the equilibrium adsorption of TC by the same biochar in brine was lower than that in pure water conditions, and the maximum adsorption q_e calculated from the fitting proved exactly the same. The maximum adsorption capacities of GBC800 predicted by the Thomas model under pure water and saltwater conditions were 16.71 mg/g and 15.47 mg/g, respectively. The errors between them and the actual measured values of 15.11 mg/g and 11.63 mg/g were 10.2% and 21.8%, respectively. Both errors were greater than 10%, which might be because the adsorption capacity of GBC800 for TC was limited and the high concentration of TC caused certain errors in the experimental results. The maximum predicted adsorption capacities of KGBC800 in pure water and saltwater were 262.01 mg/g and 230.58 mg/g, respectively. The errors between them and the experimentally calculated values of 238.37 mg/g and 211.93 mg/g were 9.02% and 8.08%, respectively. The maximum predicted adsorption capacities of N-KGBC800 in pure water and saltwater were 599.71 mg/g and 581.29 mg/g, respectively. The errors between them and the experimentally calculated values of 601.03 mg/g and 573.42 mg/g were 0.21% and 1.3%, respectively. The errors between the predicted and calculated values of the adsorption capacities of KGBC800 and N-KGBC800 for TC were both less than 10%, indicating that the Thomas model can describe the dynamic adsorption process of TC by the modified biochar in this study, and the estimated saturated adsorption capacity has a high degree of feasibility.

GBC800, KGBC800, and N-KGBC800 have the Yoon–Nelson model coefficient R^2 of absorption of TC under pure and salty water conditions, as shown in Table 8, of 0.8711, 0.9872, 0.9971, and 0.8321, respectively, and 0.9818, 0.9932, and R^2 for KGBC 800 and KGBC 800 are greater than 0.98, respectively. The parameters in the Yoon–Nelson model reflect the time required to penetrate 50% of the adhesive. GBC800 is calculated at 8.33 min and 7.89 min, respectively, in pure and saltwater conditions, whereas 50% of the absorption time is measured in 10 min. KGBC800's predicted values of 158 min and 128 min, respectively, are almost consistent with actual 50% absorbent penetration times of 150 to 160 min and 120 to 130 min. In the Yoon–Nelson model, the N-KGBC800 is 399 min and 321 min in pure and saltwater conditions, respectively, and is consistent with the values measured in actual experiments of 390 to 400 min and 320 to 330 min. The above experimental results suggest that the Yoon–Nelson adsorption model can simulate the process of this modified biocarbon dynamic absorption TC. However, because the model simplifies the actual conditions and ignores the structural characteristics of the adsorbent and the geometry of the fixed bed, there is a certain reasonable error.

4. Conclusions

(1) Using rape straw as the raw material and potassium bicarbonate ($KHCO_3$) and urea ($CO(NH_2)_2$) as the modification reagents, they were mixed in a certain proportion to form the raw pyrolysis materials. The unmodified biochar GBC800, $KHCO_3$-modified biochar KGBC800, and ($KHCO_3$)/($CO(NH_2)_2$) co-modified biochar N-KGBC800 were, respectively, prepared by the one-pot method at 800 °C. The surface of GBC800 is smooth and dense, without an obvious pore structure, and the specific surface area and total pore volume are small. After $KHCO_3$ activation, the surface of biochar KGBC800 showed an obvious coral-like three-dimensional carbon skeleton, the number of micropores and

specific surface area were significantly increased, and the adsorption performance of TC was slightly improved. However, with the addition of $KHCO_3$, the N in biochar is sharply reduced, and nitrogen-containing functional groups can be effectively introduced after urea co-pyrolysis. N-KGBC800 prepared by $KHCO_3/CO(NH_2)_2$ co-modification has a coral-like three-dimensional carbon skeleton similar to KGBC800. There are more carbon clusters, and the carbon layers have significant changes and interlayer gaps, showing a multistage porous structure. The adsorption performance of the three biochars was the best when the pH was 3~4, and the adsorption equilibrium was reached within 720 min.

(2) The kinetic models of tetracycline adsorption by the three biochar types show that they conform to the quasi-second-order kinetic model, and the adsorption process results from both physical and chemical effects. The adsorption isotherm model showed that the adsorption of tetracycline by the three biochar types was consistent with the Langmuir isotherm model, preferring monolayer adsorption, and the intermolecular force played a key role in the adsorption process. The adsorption thermodynamics showed that the adsorption of tetracycline by the three biochar was endothermic. By comparing the BET and FT-IR characterization results of GBC800, KGBC800, and N-KGBC800 before and after adsorption, the adsorption mechanisms include pore filling, electrostatic interaction, hydrogen bonds, $n-\pi$ interaction, Lewis acid–base interaction with nitrogen-containing functional groups, and $\pi-\pi$ stacking or cation $-\pi$ interaction between the aromatic ring structure of the carbon itself and TC.

(3) In the biochar fixed-bed adsorption experiment, the biochar with stronger adsorption capacity in the static adsorption performed better in the fixed-bed adsorption, and the inorganic ions in brine inhibit or interfere with the adsorption process to a certain degree, resulting in a decrease in adsorption capacity. Overall, the Thomas model and Yoon–Nelson model can describe the adsorption of tetracycline by KGBC800 and an N-KGBC800 biochar fixed bed.

Author Contributions: Conceptualization, Z.Z. and C.T.; methodology, C.T.; software, H.W.; validation, H.W. and P.G.; formal analysis, C.T., M.Z. and Z.Z.; resources, W.X. and Y.C.; data curation, M.Z.; writing—original draft preparation, C.T.; writing—review and editing, C.T.; visualization, Z.Z. and P.G.; supervision, Y.C.; project administration, Y.C. and W.X.; funding acquisition, Y.C. and W.X. All authors have read and agreed to the published version of the manuscript.

Funding: This research was funded by the open fund of the Engineering & Technology Center of Groundwater Pollution Control for Environmental Protection in Sichuan (2024-01), the open fund of the Sichuan Provincial Engineering Research Center of City Solid Waste Energy and Building Materials Conversion and Utilization Technology (No. GF2023YB002), and the Chengdu Institute of Technology 2023 Provincial Da Chuang Project (S202311116036).

Data Availability Statement: Data are available upon request from the authors.

Conflicts of Interest: Author Yiyang Chen was employed by the company Sichuan Ecology and Environment Industry Group Co., Ltd. The remaining authors declare that the research was conducted in the absence of any commercial or financial relationships that could be construed as a potential conflict of interest.

References

1. Li, J.; Wang, Z. The road to agricultural power for small farmers in large countries: Restraint and cracking. *Southwest Financ.* **2023**, *12*, 41–53.
2. Huang, L.; Zhu, Y.; Wang, Q.; Zhu, A.; Liu, Z.; Wang, Y.; Allen, D.T.; Li, L. Assessment of the effects of straw burning bans in China: Emissions, air quality, and health impacts. *Sci. Total Environ.* **2021**, *789*, 147935. [CrossRef] [PubMed]
3. Sun, Y.; Li, X.; Hu, X.; Xu, X.; Yang, W.; Sun, R.; Xue, Y.; Xu, Z. The situation, utilization status and development suggestion of rape straw resources in China. *Chin. J. Oil Crops* **2024**, 1–8. [CrossRef]
4. Li, L.; Chen, B.; Yan, G.; Gao, G.; Xu, K.; Xie, T.; Zhang, F.; Wu, X. Proposed Strategies and Current Progress of Research and Utilization of Oilseed Rape Germplasm in China. *J. Plant Genet. Resour.* **2020**, *21*, 1–19.
5. Doula, M.K.; Sarris, A.; Hliaoutakis, A.; Kydonakis, A.; Papadopoulos, N.S.; Argyriou, L. Building a strategy for soil protection at local and regional scale-the case of agricultural wastes landspreading. *Environ. Monit. Assess.* **2016**, *188*, 141. [CrossRef]

6. Li, G.; Feng, Y.; Zhu, W.; Zhang, X. Enhanced adsorptive performance of tetracycline antibiotics on lanthanum modified diatomite. *Korean J. Chem. Eng.* **2015**, *32*, 2109–2115. [CrossRef]
7. Shao, Y.; Wang, Y.; Yuan, Y.; Xie, Y. A systematic review on antibiotics misuse in livestock and aquaculture and regulation implications in China. *Sci. Total Environ.* **2021**, *798*, 149205. [CrossRef]
8. 2022 National Fishery Economic Statistical Bulletin. *Chin. Aquat. Prod.* **2023**, *8*, 7–8.
9. Zuo, R.; Peng, J.; Li, R.; Liu, S.; Wang, Y.; Wen, Q.; Hou, H.; Lu, M.; Li, Y. Progress in environmental behavior and ecotoxicology of tetracycline veterinary drugs. *Adv. Vet. Med.* **2018**, *39*, 98–101. [CrossRef]
10. Zhu, Z.; Li, L.; Xu, M.; Zhang, Q.; Hong, J. The rhomboidal flaky Fe-Mn catalyst activated persulfate for degradation of tetracycline. *Chin. Environ. Sci.* **2021**, *41*, 5142–5152. [CrossRef]
11. Wang, Z.; Bai, M.; Li, X.; Weng, L.; Ye, H. Research progress of microbial degradation of tetracycline antibiotics. *J. Agric. Environ. Sci.* **2022**, *41*, 2779–2786.
12. Zou, S.-J.; Chen, Y.-F.; Zhang, Y.; Wang, X.-F.; You, N.; Fan, H.-T. A hybrid sorbent of α-iron oxide/reduced graphene oxide: Studies for adsorptive removal of tetracycline antibiotics. *J. Alloys Compd.* **2021**, *863*, 158475. [CrossRef]
13. Chen, K.; Huang, D. Application of various adsorbent materials in removal of tetracycline antibiotic residues in water. *J. Guangxi Med. Univ.* **2018**, *35*, 1169–1172. [CrossRef]
14. Du, C.; Wu, T.; Hu, T.; Liu, Y.; Deng, J. Preparation of biochar by ball milling and its adsorption of methylene blue. *J. Sichuan Univ. Arts Sci.* **2023**, *33*, 21–25.
15. Zhang, T.; Yang, Y.; Li, W.; Zhou, Y.; Wu, L.; Cheng, Z. Adsorption of tetracycline by alkali-modified biochar. *J. Yichun Univ.* **2022**, *44*, 6–12+47.
16. Sun, Y.; Zheng, L.; Zheng, X.; Xiao, D.; Yang, Y.; Zhang, Z.; Ai, B.; Sheng, Z. Adsorption of Sulfonamides in Aqueous Solution on Reusable Coconut-Shell Biochar Modified by Alkaline Activation and Magnetization. *Front. Chem.* **2022**, *9*, 814647. [CrossRef]
17. Che, H.; Wei, G.; Fan, Z.; Zhu, Y.; Zhang, L.; Wei, Z.; Huang, X.; Wei, L. Super facile one-step synthesis of sugarcane bagasse derived N-doped porous biochar for adsorption of ciprofloxacin. *J. Environ. Manag.* **2023**, *335*, 117566. [CrossRef]
18. Lu, S.; Huang, X.; Tang, M.; Peng, Y.; Wang, S.; Makwarimba, C.P. Synthesis of N-doped hierarchical porous carbon with excellent toluene adsorption properties and its activation mechanism. *Environ. Pollut.* **2021**, *284*, 117113. [CrossRef]
19. Li, H.; Tang, M.; Huang, X.; Wang, L.; Liu, Q.; Lu, S. An efficient biochar adsorbent for CO_2 capture: Combined experimental and theoretical study on the promotion mechanism of N-doping. *Chem. Eng. J.* **2023**, *466*, 143095. [CrossRef]
20. Chen, X.; Oh, W.-D.; Hu, Z.-T.; Sun, Y.-M.; Webster, R.D.; Li, S.-Z.; Lim, T.-T. Enhancing sulfacetamide degradation by peroxymonosulfate activation with N-doped graphene produced through delicately-controlled nitrogen functionalization via tweaking thermal annealing processes. *Appl. Catal. B-Environ.* **2018**, *225*, 243–257. [CrossRef]
21. Cheng, Y.; Wang, B.; Shen, J.; Yan, P.; Kang, J.; Wang, W.; Bi, L.; Zhu, X.; Li, Y.; Wang, S.; et al. Preparation of novel N-doped biochar and its high adsorption capacity for atrazine based on π–π electron donor-acceptor interaction. *J. Hazard. Mater.* **2022**, *432*, 128757. [CrossRef] [PubMed]
22. Obanla, O.R.; Hestekin, J.A.; Ojewumi, M.E.; Bousrih, I.; Fawole, M.C. Enhancing rubber (*Hevea brasiliensis*) seed shell biochar through acid-base modification for effective phenol removal from aqueous environments. *Results Eng.* **2023**, *20*, 15. [CrossRef]
23. Huang, Y.; Li, K.; Yao, W.; Gao, Y. Factors affecting the pore structure and adsorption performance of rice straw carbon prepared by potassium bicarbonate activation. *Environ. Chem.* **2018**, *37*, 569–575.
24. Tian, W.; Zhang, H.; Sun, H.; Tade, M.O.; Wang, S. Template-free synthesis of N-doped carbon with pillared-layered pores as bifunctional materials for supercapacitor and environmental applications. *Carbon* **2017**, *118*, 98–105. [CrossRef]
25. Li, Y.; Xing, B.; Wang, X.; Wang, K.; Zhu, L.; Wang, S. Nitrogen-Doped Hierarchical Porous Biochar Derived from Corn Stalks for Phenol-Enhanced Adsorption. *Energy Fuels* **2019**, *33*, 12459–12468. [CrossRef]
26. Yim, S.D.; Kim, S.J.; Baik, J.H.; Nam, I.S.; Mok, Y.S.; Lee, J.H.; Cho, B.K.; Oh, S.H. Decomposition of urea into NH_3 for the SCR process. *Ind. Eng. Chem. Res.* **2004**, *43*, 4856–4863. [CrossRef]
27. Li, K.; Chen, W.; Yang, H.; Chen, Y.; Xia, S.; Xia, M.; Tu, X.; Chen, H. Mechanism of biomass activation and ammonia modification for nitrogen-doped porous carbon materials. *Bioresour. Technol.* **2019**, *280*, 260–268. [CrossRef]
28. Chen, W.; Yang, H.P.; Chen, Y.Q.; Chen, X.; Fang, Y.; Chen, H.P. Biomass pyrolysis for nitrogen-containing liquid chemicals and nitrogen-doped carbon materials. *J. Anal. Appl. Pyrolysis* **2016**, *120*, 186–193. [CrossRef]
29. Al-Ghouti, M.A.; Da'ana, D.A. Guidelines for the use and interpretation of adsorption isotherm models: A review. *J. Hazard. Mater.* **2020**, *393*, 122383. [CrossRef]
30. Duan, X.; Sun, H.; Kang, J.; Wang, Y.; Indrawirawan, S.; Wang, S. Insights into Heterogeneous Catalysis of Persulfate Activation on Dimensional-Structured Nanocarbons. *ACS Catal.* **2015**, *5*, 4629–4636. [CrossRef]
31. Chen, J.; Yang, J.; Hu, G.; Hu, X.; Li, Z.; Shen, S.; Radosz, M.; Fan, M. Enhanced CO_2 Capture Capacity of Nitrogen-Doped Biomass-Derived Porous Carbons. *ACS Sustain. Chem. Eng.* **2016**, *4*, 1439–1445. [CrossRef]
32. Ying, Z.W.; Chen, X.W.; Li, H.; Liu, X.Q.; Zhang, C.; Zhang, J.; Yi, G.F. Efficient Adsorption of Methylene Blue by Porous Biochar Derived from Soybean Dreg Using a One-Pot Synthesis Method. *Molecules* **2021**, *26*, 661. [CrossRef]
33. Huang, W.; Zhang, X.P.; Zhang, J.Q.; Tang, Y.X.; Luo, Z. Preparation of magnetically modified sheep manure-derived ZVI-biochar and characterization of its activation over monosulfate for AO7 degradation. *J. Environ. Sci. Eng.* **2022**, *42*, 196–208. [CrossRef]
34. Yu, H.X.; Gu, L.; Chen, L.; Wen, H.F.; Zhang, D.F.; Tao, H. Activation of grapefruit derived biochar by its peel extracts and its performance for tetracycline removal. *Bioresour. Technol.* **2020**, *316*, 123971. [CrossRef] [PubMed]

35. Li, S.C.; Du, G.Y.; Hu, Z.H.; Zhang, H.T. Preparation of nitrogen-doped biochar and its adsorption characteristics on heavy metal lead in water. *New Chem. Mater.* **2023**, *51*, 214–220. [CrossRef]
36. Kang, Y.X.; Kang, X.; Li, D.P.; Sun, Z.Y.; Song, X.S.; Zhao, X.X. Adsorption properties of pigeon feces biochar prepared at different pyrolysis temperatures on methicillin in water. *J. Donghua Univ.* **2021**, *47*, 100–108. [CrossRef]
37. Zhang, S.; Yang, X.; Liu, L.; Ju, M.; Zheng, K. Adsorption Behavior of Selective Recognition Functionalized Biochar to Cd(II) in Wastewater. *Materials* **2018**, *11*, 299. [CrossRef]
38. Zhao, X.L.; Yang, L.N.; Wang, Y.; Dong, N. Adsorption removal of imidacloprid from water by biochar from tobacco stalks. *Appl. Chem.* **2024**, *53*, 308–313+318. [CrossRef]
39. Jang, H.M.; Kan, E. A novel hay-derived biochar for removal of tetracyclines in water. *Bioresour. Technol.* **2019**, *274*, 162–172. [CrossRef]
40. Xiang, Y.J.; Xu, Z.Y.; Wei, Y.Y.; Zhou, Y.Y.; Yang, X.; Yang, Y.; Yang, J.; Zhang, J.C.; Luo, L.; Zhou, Z. Carbon-based materials as adsorbent for antibiotics removal: Mechanisms and influencing factors. *J. Environ. Manag.* **2019**, *237*, 128–138. [CrossRef]
41. Chen, J.; Li, X.; Li, B.; Sun, X.; Huang, W.; Lu, Y. Study on adsorption performance of rape straw biochar to water methylene blue. *Water Treat. Technol.* **2022**, *48*, 37–42+47. [CrossRef]
42. Li, H.; Hu, J.; Meng, Y.; Su, J.; Wang, X. An investigation into the rapid removal of tetracycline using multilayered graphene-phase biochar derived from waste chicken feather. *Sci. Total Environ.* **2017**, *603*, 39–48. [CrossRef] [PubMed]
43. Deng, Y.; She, A.L.; Zhang, Y.; Ni, F.Q.; Ao, T.Q.; Chen, W.Q. Effect of pyrolysis temperature on carbon structure, ash content and adsorption of tetracycline on corn kernel biochar. *J. Agric. Environ. Sci.* **2024**, 1–18.
44. Liu, S.; Li, J.; Xu, S.; Wang, M.; Zhang, Y.; Xue, X. A modified method for enhancing adsorption capability of banana pseudostem biochar towards methylene blue at low temperature. *Bioresour. Technol.* **2019**, *282*, 48–55. [CrossRef]
45. Guo, X.; Wang, J. A general kinetic model for adsorption: Theoretical analysis and modeling. *J. Mol. Liq.* **2019**, *288*, 111100. [CrossRef]
46. Wang, J.; Guo, X. Adsorption kinetic models: Physical meanings, applications, and solving methods. *J. Hazard. Mater.* **2020**, *390*, 122156. [CrossRef]
47. Ho, Y.S.; Wase, D.A.J.; Forster, C.F. Removal of lead ions from aqueous solution using sphagnum moss peat as adsorbent. *Water SA* **1996**, *22*, 219–224.
48. Liu, H.; Xu, G.; Li, G. Preparation of porous biochar based on pharmaceutical sludge activated by NaOH and its application in the adsorption of tetracycline. *J. Colloid Interface Sci.* **2021**, *587*, 271–278. [CrossRef]
49. Yu, W.; Lian, F.; Cui, G.; Liu, Z. N-doping effectively enhances the adsorption capacity of biochar for heavy metal ions from aqueous solution. *Chemosphere* **2018**, *193*, 8–16. [CrossRef]
50. Lian, F.; Cui, G.; Liu, Z.; Duo, L.; Zhang, G.; Xing, B. One-step synthesis of a novel N-doped microporous biochar derived from crop straws with high dye adsorption capacity. *J. Environ. Manag.* **2016**, *176*, 61–68. [CrossRef]
51. Hao, Z.; Wang, C.; Yan, Z.; Jiang, H.; Xu, H. Magnetic particles modification of coconut shell-derived activated carbon and biochar for effective removal of phenol from water. *Chemosphere* **2018**, *211*, 962–969. [CrossRef]
52. Liu, L.; Deng, G.; Shi, X. Adsorption characteristics and mechanism of p-nitrophenol by pine sawdust biochar samples produced at different pyrolysis temperatures. *Sci. Rep.* **2020**, *10*, 5149. [CrossRef]
53. Fierro, V.; Torne-Fernandez, V.; Montane, D.; Celzard, A. Adsorption of phenol onto activated carbons having different textural and surface properties. *Microporous Mesoporous Mater.* **2008**, *111*, 276–284. [CrossRef]
54. Zhang, P.; Li, Y.; Cao, Y.; Han, L. Characteristics of tetracycline adsorption by cow manure biochar prepared at different pyrolysis temperatures. *Bioresour. Technol.* **2019**, *285*, 121348. [CrossRef]
55. Cui, J.T.; Zhang, M.Y.; Mi, M.; Zhao, Y.M.; Jin, Z.W.; Wong, M.H.; Shan, S.D.; Ping, L.F. Effects of swine manure and straw biochars on fluorine adsorption-desorption in soils. *PLoS ONE* **2024**, *19*, 21. [CrossRef] [PubMed]
56. Dai, J.; Meng, X.; Zhang, Y.; Huang, Y. Effects of modification and magnetization of rice straw derived biochar on adsorption of tetracycline from water. *Bioresour. Technol.* **2020**, *311*, 123455. [CrossRef] [PubMed]
57. Nandhakumar, V.; Elavarasan, A.; Chandramohan, M.; Balasuramanian, N. Kinetics and isotherm studies on the adsorption of hexavalent chromium onto phosphoric acid activated *Mimusops elengi* leaves carbon. *Int. J. Curr. Res. Chem. Pharm. Sci.* **2017**, *4*, 67–76. [CrossRef]
58. Garba, Z.N.; Lawan, I.; Zhou, W.; Zhang, M.; Wang, L.; Yuan, Z. Microcrystalline cellulose (MCC) based materials as emerging adsorbents for the removal of dyes and heavy metals—A review. *Sci. Total Environ.* **2020**, *717*, 135070. [CrossRef] [PubMed]
59. Srivastava, V.C.; Swamy, M.M.; Mall, I.D.; Prasad, B.; Mishra, I.M. Adsorptive removal of phenol by bagasse fly ash and activated carbon: Equilibrium, kinetics and thermodynamics. *Colloids Surf. A Physicochem. Eng. Asp.* **2006**, *272*, 89–104. [CrossRef]
60. Sun, A.H.; Bian, S.Y.; Li, L.Z.; Guo, Z.J.; Li, W.J.; Li, J.H.; Xu, S.Y.; Liu, P.D. Preparation of highly adsorptive biochar by sequential iron impregnation under refluxing and pyrolysis at low temperature for removal of tetracycline. *Environ. Pollut.* **2024**, *348*, 10. [CrossRef]
61. Kamali, M.; Appels, L.; Kwon, E.E.; Aminabhavi, T.M.; Dewil, R. Biochar in water and wastewater treatment-a sustainability assessment. *Chem. Eng. J.* **2021**, *420*, 129946. [CrossRef]
62. Chen, Y.; Liu, J.; Zeng, Q.; Liang, Z.; Ye, X.; Lv, Y.; Liu, M. Preparation of *Eucommia ulmoides* lignin-based high-performance biochar containing sulfonic group: Synergistic pyrolysis mechanism and tetracycline hydrochloride adsorption. *Bioresour. Technol.* **2021**, *329*, 124856. [CrossRef]

63. Yu, K.; Chen, Y.X.; Wang, C.B.; Sun, D.; Shen, Q. Adsorption performance of hydrothermal bamboo biochar on tetracycline hydrochloride. *J. Huzhou Norm. Univ.* **2021**, *43*, 54–58.
64. Sewu, D.D.; Jung, H.; Kim, S.S.; Lee, D.S.; Woo, S.H. Decolorization of cationic and anionic dye-laden wastewater by steam-activated biochar produced at an industrial-scale from spent mushroom substrate. *Bioresour. Technol.* **2019**, *277*, 77–86. [CrossRef] [PubMed]
65. Ndoun, M.C.; Elliott, H.A.; Preisendanz, H.E.; Williams, C.F.; Knopf, A.; Watson, J.E. Adsorption of pharmaceuticals from aqueous solutions using biochar derived from cotton gin waste and guayule bagasse. *Biochar* **2021**, *3*, 89–104. [CrossRef]
66. He, L.; Liu, F.-f.; Zhao, M.; Qi, Z.; Sun, X.; Afzal, M.Z.; Sun, X.; Li, Y.; Hao, J.; Wang, S. Electronic-property dependent interactions between tetracycline and graphene nanomaterials in aqueous solution. *J. Environ. Sci.* **2018**, *66*, 286–294. [CrossRef]
67. Zheng, H.; Wang, Z.; Zhao, J.; Herbert, S.; Xing, B. Sorption of antibiotic sulfamethoxazole varies with biochars produced at different temperatures. *Environ. Pollut.* **2013**, *181*, 60–67. [CrossRef] [PubMed]
68. Zhang, D.; He, Q.; Hu, X.; Zhang, K.; Chen, C.; Xue, Y. Enhanced adsorption for the removal of tetracycline hydrochloride (TC) using ball-milled biochar derived from crayfish shell. *Colloids Surf. A Physicochem. Eng. Asp.* **2021**, *615*, 126254. [CrossRef]
69. Xu, Z.; Cai, J.-G.; Pan, B.-C. Mathematically modeling fixed-bed adsorption in aqueous systems. *J. Zhejiang Univ.-Sci. A* **2013**, *14*, 155–176. [CrossRef]
70. Lin, J.; Zhan, Y.; Wang, H.; Chu, M.; Wang, C.; He, Y.; Wang, X. Effect of calcium ion on phosphate adsorption onto hydrous zirconium oxide. *Chem. Eng. J.* **2017**, *309*, 118–129. [CrossRef]
71. Zhao, J.; Gao, F.; Sun, Y.; Fang, W.; Li, X.; Dai, Y. New use for biochar derived from bovine manure for tetracycline removal. *J. Environ. Chem. Eng.* **2021**, *9*, 105585. [CrossRef]
72. Kumar, P.A.; Chakraborty, S. Fixed-bed column study for hexavalent chromium removal and recovery by short-chain polyaniline synthesized on jute fiber. *J. Hazard. Mater.* **2009**, *162*, 1086–1098. [CrossRef] [PubMed]
73. Dolatyari, L.; Yaftian, M.R.; Rostamnia, S. Adsorption of Th(IV) and U(VI) on functionalized SBA-15 mesoporous silica materials using fixed bed column method; breakthrough curves prediction and modeling. *Sep. Sci. Technol.* **2018**, *53*, 1282–1294. [CrossRef]
74. Hasan, S.H.; Ranjan, D.; Talat, M. Agro-industrial waste 'wheat bran' for the biosorptive remediation of selenium through continuous up-flow fixed-bed column. *J. Hazard. Mater.* **2010**, *181*, 1134–1142. [CrossRef]
75. Wang, L.; Feng, J.J.; Tao, M.L. Dynamic adsorption of dyes by quaternary ammonium ionized acrylic fibers. *Chem. Ind. Eng.* **2020**, *37*, 73–79. [CrossRef]